

01 Dec 2014

Understanding Higher-Order Nonlocal Halo Bias at Large Scales by Combining the Power Spectrum with the Bispectrum

Shun Saito

Missouri University of Science and Technology, saitos@mst.edu

Tobias Baldauf

For full list of authors, see publisher's website.

Follow this and additional works at: https://scholarsmine.mst.edu/phys_facwork

 Part of the [Physics Commons](#)

Recommended Citation

S. Saito et al., "Understanding Higher-Order Nonlocal Halo Bias at Large Scales by Combining the Power Spectrum with the Bispectrum," *Physical Review D - Particles, Fields, Gravitation and Cosmology*, vol. 90, no. 12, American Physical Society (APS), Dec 2014.

The definitive version is available at <https://doi.org/10.1103/PhysRevD.90.123522>

This Article - Journal is brought to you for free and open access by Scholars' Mine. It has been accepted for inclusion in Physics Faculty Research & Creative Works by an authorized administrator of Scholars' Mine. This work is protected by U. S. Copyright Law. Unauthorized use including reproduction for redistribution requires the permission of the copyright holder. For more information, please contact scholarsmine@mst.edu.



Understanding higher-order nonlocal halo bias at large scales by combining the power spectrum with the bispectrum

Shun Saito,^{1,*} Tobias Baldauf,² Zvonimir Vlah,³ Uroš Seljak,^{4,5} Teppei Okumura,¹ and Patrick McDonald⁵

¹*Kavli Institute for the Physics and Mathematics of the Universe (WPI),*

Todai Institutes for Advanced Study, The University of Tokyo, Chiba 277-8582, Japan

²*School of Natural Sciences, Institute for Advanced Study, 1 Einstein Drive, Princeton, New Jersey 08540, USA*

³*Physik Institut, University of Zürich, Winterthurerstrasse 190, CH-8057 Zürich, Switzerland*

⁴*Department of Physics, University of California, Berkeley, California 94720, USA*

⁵*Lawrence Berkeley National Laboratory, Physics Department, Berkeley, California 94720, USA*

(Received 1 October 2014; published 16 December 2014)

Understanding the relation between underlying matter distribution and biased tracers such as galaxies or dark matter halos is essential to extract cosmological information from ongoing or future galaxy redshift surveys. At sufficiently large scales such as the baryon acoustic oscillation (BAO) scale, a standard approach for the bias problem on the basis of the perturbation theory (PT) is to assume the “local bias” model in which the density field of biased tracers is deterministically expanded in terms of matter density field at the same position. The higher-order bias parameters are then determined by combining the power spectrum with higher-order statistics such as the bispectrum. As is pointed out by recent studies, however, nonlinear gravitational evolution naturally induces nonlocal bias terms even if initially starting only with purely local bias. As a matter of fact, previous works showed that the second-order nonlocal bias term, which corresponds to the gravitational tidal field, is important to explain the characteristic scale-dependence of the bispectrum. In this paper we extend the nonlocal bias term up to third order, and investigate whether the PT-based model including nonlocal bias terms can simultaneously explain the power spectrum and the bispectrum of simulated halos in N -body simulations. The bias renormalization procedure ensures that only one additional term is necessary to be introduced to the power spectrum as a next-to-leading order correction, even if third-order nonlocal bias terms are taken into account. We show that the power spectrum, including density and momentum, and the bispectrum between halo and matter in N -body simulations can be simultaneously well explained by the model including up to third-order nonlocal bias terms at $k \lesssim 0.1h/\text{Mpc}$. Also, the results are in a good agreement with theoretical predictions of a simple coevolution picture, although the agreement is not perfect. These trend can be found for a wide range of halo mass, $0.7 \lesssim M_{\text{halo}} [10^{13} M_{\odot}/h] \lesssim 20$ at various redshifts, $0 \leq z \leq 1$. These demonstrations clearly show a failure of the local bias model even at such large scales, and we conclude that nonlocal bias terms should be consistently included in order to accurately model statistics of halos.

DOI: [10.1103/PhysRevD.90.123522](https://doi.org/10.1103/PhysRevD.90.123522)

PACS numbers: 98.65.Dx, 95.35.+d, 98.80.Es

I. INTRODUCTION

Precise observation of the early universe has been well established by measurements of temperature and polarization anisotropy of the cosmic microwave background (CMB) such as Wilkinson Microwave Anisotropy Probe (WMAP) [1–3] or Planck [4]. Now we enter a new era of precision cosmology by getting in hand various kinds of large-scale structure measurements in late-time universe, mainly aiming at unveiling dark universe (see [5] for a recent review). In particular, clustering of galaxies in a three dimensional map of the Universe offers us a lot of fruitful cosmological information via the baryon acoustic oscillations (BAOs), redshift-space distortion (RSD), or the shape

of galaxy clustering statistics such as the power spectrum and the bispectrum (for an encompassing review, see [6]). As a matter of fact, recent works by Baryon Oscillation Spectroscopic Survey (BOSS) [7] in Sloan Digital Sky Survey III (SDSS-III) [8] or WiggleZ survey [9] have already accomplished very accurate measurements of such signals [10–24]. Planned or near-future galaxy redshift surveys, which include Subaru Prime Focus Spectrograph (PFS) Survey [25], Hobby-Eberly Telescope Dark Energy Experiment (HETDEX) [26], Dark Energy Spectroscopic Instrument (DESI) [27] and Euclid [28], will continue to improve measurement accuracy at various redshift and scales.

In order to unlock the full potential of cosmological information in the galaxy clustering, it is essential to understand the relation between underlying matter

*shun.saito@ipmu.jp

distribution and galaxies, known as the so-called galaxy bias problem. It is often assumed that galaxy distribution well traces underlying matter distribution which can be directly probed by cosmological N -body simulations. Given the fact that we do not have complete knowledge of galaxy formation scenario in nonlinear structure formation, it is a common practice to connect observed galaxy distribution to simulated dark matter halos. This approach is based on the halo model [29,30], and its associated techniques such as halo occupation distribution (HOD) and subhalo abundance matching (SHAM) (e.g., [31–34]) are applied to somewhat small-scale galaxy clustering (typically $\sim \mathcal{O}(0.1\text{--}10)$ Mpc) (see e.g., [35–37] and references therein for recent studies).

Even though dark matter halos can be easily constructed in N -body simulations, it is important to theoretically understand clustering of the halos, or halo bias, especially at large scales around BAOs (~ 150 Mpc), because the halo clustering is sensitive to underlying cosmology at the regimes (where, in other words, the two-halo term is dominant in the halo-model context). Some authors tried to formulate the halo or galaxy bias in parametric ways (see e.g., [38–41]) and showed a successful performance depending on their specific purpose, although it might be hard to be justified in more general situations. It is therefore desirable to develop an analytic formulation to describe the halo clustering in a physically-well motivated way. Perturbation theory (PT) is a natural approach along this direction, and, in the PT approach, the so-called “local bias” model [42,43] in which the density field of halos is deterministically Taylor-expanded in terms of matter density field at the same position as

$$\delta_h(\mathbf{x}) = \sum_n \frac{b_n}{n!} \delta_m(\mathbf{x})^n, \quad (1)$$

where b_n is the bias coefficient at n th order, and δ_h and δ_m describes density fields of halos and matter, respectively. It is well known that the local bias model works well at linear order to some extent [42], and the fitting formula for the halo mass function is calibrated so that it also consistently reproduces the linear bias value in simulations [44,45]. However, a couple of issues in the model have been recently pointed out. First of all, the model prefers different values of nonlinear bias parameter like b_2 for the halo power spectrum and the bispectrum [46,47], although the model looks well fitted to the spectra by properly choosing nonlinear bias parameters (see e.g., [48–50]). In addition, the authors [51–54] show that nonlinear gravitational evolution naturally induces nonlocal terms, and there are clear evidences of such a term at least at second-order perturbation observed in the bispectrum in simulations [53,54]. These caveats clearly warn adopting the local bias model from a physical point of view.

In this paper we continue to study how well the bias model including nonlocal terms performs against the halo statistics in N -body simulations. In particular, we focus on

how well such a model can simultaneously explain the power spectrum as well as the bispectrum which again cannot be realized in the simple local bias model. While the leading-order (i.e., tree-level) bispectrum requires only up to second-order perturbation, it is necessary to consider up to third order as a next-to-leading order correction in the power spectrum. The author [55] showed that the bias renormalization procedure allows us to write down a *physical* expression for the halo statistics and the third-order local bias term is absorbed into the linear bias. As we will revisit later, Ref. [51] shows that all the correction terms associated with the third-order nonlocal bias can be summarized into only one term. This bias renormalization approach has been recently readdressed in terms of the effective field theory by [56], and they also reached the same conclusion (see also [57]). Thus we have in hand a very simple bias model on the basis of PT even if considering all the local and nonlocal terms up to third order. Then the natural question that arises is whether the simple bias model can well explain the simulated halo power spectrum as well, and also whether the fitted value of the bias parameter is consistent with what is physically expected. In order to answer these questions, we study the halo-matter statistics in a standard Λ CDM universe at a various halo-mass range and redshift. We jointly fit the PT model to the power spectrum together with the bispectrum. An advantage of focusing on the halo-matter statistics is that it is free from the stochastic bias [58,59] and the velocity bias [60–63]. We also investigate the cross spectrum between halo density and matter momentum which was recently studied in modeling the RSDs in the Distribution Function approach (see [64–69] for a series of papers) and should be simultaneously explained by the same bias values if the model works.

The outline of this paper is as follows. In Sec. II, we first revisit the argument in [51] and summarize a model to describe the halo-matter power spectrum and the bispectrum including nonlocal terms up to third order. In particular, we extend the model to the cross power spectrum between halo density and matter momentum which can be easily measured from the simulations and can be used to study the bias model as well. In addition, we study a simple coevolution picture of dark matter and halo fluids and derive a third-order solution. In Sec. III we describe our simulation details and fitting procedure. We then show our results in Sec. IV in which the bias model is compared with halo-matter power spectra in detail. Finally we make a summary and conclusion in in Sec. V.

II. THE HALO-MATTER CROSS STATISTICS IN THE PRESENCE OF NONLOCAL BIAS TERMS

In this section we explicitly write down expressions for the halo-matter power spectrum on the basis of the perturbation theory (PT), including nonlocal bias terms. For this purpose we revisit an procedure proposed by [51]

in which all the possible bias terms are introduced by symmetry arguments and can be properly renormalized. After we review exactly the same procedure in [51] for the matter-density and halo-density power spectrum, we will extend it to the matter-momentum and halo-density cross spectrum and bias renormalization [53]. For readers unfamiliar with PT, we refer to Appendix A, where basic equations in the PT formalism and our notations are summarized. While

we here focus on the cross power spectrum, we present expressions for the autocorrelators in Appendix A as well.

A. The halo-matter density power spectrum

Starting from Eq. (A10) which includes all possible perturbations up to third order for the next-to-leading order calculation of the power spectrum (e.g., see [6]), the matter-halo density power spectrum is written as

$$\begin{aligned}
 P_{00}^{\text{hm}}(k) = & c_\delta P(k) + c_\delta P_{\delta\delta}^{(13)}(k) + c_\delta P_{\delta\delta}^{(22)}(k) + \frac{34}{21} c_{\delta^2} \sigma^2 P(k) + \frac{1}{2} c_{\delta^3} \sigma^2 P(k) + \frac{1}{3} c_{\delta s^2} \sigma^2 P(k) + \frac{1}{2} c_{\delta \epsilon^2} \sigma_e^2 P(k) \\
 & + c_{\delta^2} \int \frac{d^3 q}{(2\pi)^3} P(q) P(|\mathbf{k} - \mathbf{q}|) F_S^{(2)}(\mathbf{q}, \mathbf{k} - \mathbf{q}) + c_{s^2} \int \frac{d^3 q}{(2\pi)^3} P(q) P(|\mathbf{k} - \mathbf{q}|) F_S^{(2)}(\mathbf{q}, \mathbf{k} - \mathbf{q}) S^{(2)}(\mathbf{q}, \mathbf{k} - \mathbf{q}) \\
 & + 2c_{s^2} P(k) \int \frac{d^3 q}{(2\pi)^3} P(q) F_S^{(2)}(-\mathbf{q}, \mathbf{k}) S^{(2)}(\mathbf{q}, \mathbf{k} - \mathbf{q}) + 2c_{st} P(k) \int \frac{d^3 q}{(2\pi)^3} P(q) D_S^{(2)}(-\mathbf{q}, \mathbf{k}) S^{(2)}(\mathbf{q}, \mathbf{k} - \mathbf{q}) \\
 & + 2c_\psi P(k) \int \frac{d^3 q}{(2\pi)^3} P(q) \left[\frac{3}{2} D_S^{(3)}(\mathbf{q}, -\mathbf{q}, -\mathbf{k}) - 2F_S^{(2)}(-\mathbf{q}, \mathbf{k}) D_S^{(2)}(\mathbf{q}, \mathbf{k} - \mathbf{q}) \right], \tag{2}
 \end{aligned}$$

where the superscript ‘‘h’’ stands for a quantity for halos and the subscript ‘‘0’’ stands for the zeroth moment of mass-weighted velocity. All the bias coefficients, c_n , are bare bias parameters, and do not necessarily have clear physical meaning as explained later. $P(k)$ denotes the linear matter power spectrum, and the r.m.s of the fluctuated matter field, σ^2 , is defined by $\sigma^2 \equiv \int q^2 dq P(q)/(2\pi^2)$. Note that the term involving the third-order tidal term, s^3 , vanishes in this case. Reference [55] argued that the first and second lines in Eq. (2) can be renormalized to a *physical* linear bias as follows: in the limit of $k \rightarrow 0$, one finds

$$\begin{aligned}
 c_\delta P(k) + c_\delta P_{\delta\delta}^{(13)}(k) + c_\delta P_{\delta\delta}^{(22)}(k) + \frac{34}{21} c_{\delta^2} \sigma^2 P(k) \\
 + \frac{1}{2} c_{\delta^3} \sigma^2 P(k) + \frac{1}{3} c_{\delta s^2} \sigma^2 P(k) + \frac{1}{2} c_{\delta \epsilon^2} \sigma_e^2 P(k) \\
 \xrightarrow{k \rightarrow 0} \left(c_\delta + \frac{34}{21} c_{\delta^2} \sigma^2 + \frac{1}{2} c_{\delta^3} \sigma^2 + \frac{1}{3} c_{\delta s^2} \sigma^2 + \frac{1}{2} c_{\delta \epsilon^2} \sigma_e^2 \right) P(k). \tag{3}
 \end{aligned}$$

In the limit of $k \rightarrow 0$, all the terms proportional to $P(k)$ should behave as the linear bias parameter times the linear power spectrum $P(k)$, which means that all the terms in the bracket can be interpreted as a renormalized linear bias. The third-order local bias term, c_{δ^3} , is thus renormalized into the linear bias and not necessary to be considered. Reference [51] further found that the fifth, sixth and seventh lines in Eq. (2), whose origins are the third-order nonlocal terms, can be renormalized in a similar manner into a linear bias and *just one* additional bias parameter. In order to see this, let us first separate out $k \rightarrow 0$ limit of these terms,

$$\int \frac{d^3 q}{(2\pi)^3} P(q) F_S^{(2)}(-\mathbf{q}, \mathbf{k}) S^{(2)}(\mathbf{q}, \mathbf{k} - \mathbf{q}) \rightarrow \frac{34}{63} \sigma^2, \tag{4}$$

$$\begin{aligned}
 \int \frac{d^3 q}{(2\pi)^3} P(q) D_S^{(2)}(-\mathbf{q}, \mathbf{k}) S^{(2)}(\mathbf{q}, \mathbf{k} - \mathbf{q}) \rightarrow -\frac{8}{63} \sigma^2, \tag{5} \\
 \int \frac{d^3 q}{(2\pi)^3} P(q) \\
 \times \left[\frac{3}{2} D_S^{(3)}(\mathbf{q}, -\mathbf{q}, -\mathbf{k}) - 2F_S^{(2)}(-\mathbf{q}, \mathbf{k}) D_S^{(2)}(\mathbf{q}, \mathbf{k} - \mathbf{q}) \right] \rightarrow 0. \tag{6}
 \end{aligned}$$

These terms thus behaves as constants at $k \rightarrow 0$ and hence can be renormalized to linear bias parameters just as Eq. (3). In addition, Ref. [51] found that these integrals exactly match each other and behaves as a filter function, once constants in $k \rightarrow 0$ limit are separated out and normalization factors are properly chosen,

$$\begin{aligned}
 \int \frac{d^3 q}{(2\pi)^3} P(q) F_S^{(2)}(-\mathbf{q}, \mathbf{k}) S^{(2)}(\mathbf{q}, \mathbf{k} - \mathbf{q}) \\
 = -\frac{8}{21} \sigma_3^2(k) + \frac{34}{63} \sigma^2, \tag{7}
 \end{aligned}$$

$$\begin{aligned}
 \int \frac{d^3 q}{(2\pi)^3} P(q) D_S^{(2)}(-\mathbf{q}, \mathbf{k}) S^{(2)}(\mathbf{q}, \mathbf{k} - \mathbf{q}) \\
 = \frac{16}{105} \sigma_3^2(k) - \frac{8}{63} \sigma^2, \tag{8}
 \end{aligned}$$

$$\begin{aligned}
 \int \frac{d^3 q}{(2\pi)^3} P(q) \\
 \times \left[\frac{3}{2} D_S^{(3)}(\mathbf{q}, -\mathbf{q}, -\mathbf{k}) - 2F_S^{(2)}(-\mathbf{q}, \mathbf{k}) D_S^{(2)}(\mathbf{q}, \mathbf{k} - \mathbf{q}) \right] \\
 = \frac{256}{2205} \sigma_3^2(k), \tag{9}
 \end{aligned}$$

where we define $\sigma_3^2(k)$ as

$$\sigma_3^2(k) \equiv k^3 \int \frac{r^2 dr}{2\pi^2} P(kr) I_R(r). \quad (10)$$

For instance in the case of Eq. (7), $I_R(r)$ is described as,

$$I_R(r) = \frac{5}{128r^4} (1+r^2)(-3+14r^2-3r^4) + \frac{3(r^2-1)^4}{256r^5} \ln \left| \frac{1+r}{1-r} \right|. \quad (11)$$

$I_R(r)$ is the filtering function satisfying $I_R(r) \rightarrow 1$ at $r \rightarrow 0$ and $I_R(r) \rightarrow 0$ at $r \rightarrow \infty$ (see Fig. 2 in [51]). Again, these three terms end up with a constant plus the $\sigma_3^2(k)$ term even though the functional forms of this filtering function for each term are all different. Based upon the considerations above all, one finds an expression for the halo-matter density power spectrum

$$\begin{aligned} P_{00}^{\text{hm}}(k) &= \left(c_\delta + \frac{34}{21} c_{\delta^2} \sigma^2 + \frac{1}{2} c_{\delta^3} \sigma^2 + \frac{1}{3} c_{\delta s^2} \sigma^2 + \frac{1}{2} c_{\delta e^2} \sigma_e^2 + \frac{68}{63} c_{s^2} \sigma^2 - \frac{16}{63} c_{st} \sigma^2 \right) P_{\delta\delta}^{\text{NL}}(k) \\ &\quad + c_{\delta^2} \int \frac{d^3 q}{(2\pi)^3} P(q) P(|\mathbf{k}-\mathbf{q}|) F_S^{(2)}(\mathbf{q}, \mathbf{k}-\mathbf{q}) + c_{s^2} \int \frac{d^3 q}{(2\pi)^3} P(q) P(|\mathbf{k}-\mathbf{q}|) F_S^{(2)}(\mathbf{q}, \mathbf{k}-\mathbf{q}) S^{(2)}(\mathbf{q}, \mathbf{k}-\mathbf{q}) \\ &\quad + \left(-\frac{16}{21} c_{s^2} + \frac{32}{105} c_{st} + \frac{512}{2205} c_\psi \right) \sigma_3^2(k) P(k) \\ &= b_1 P_{\delta\delta}^{\text{NL}}(k) + b_2 P_{b_2, \delta}(k) + b_{s^2} P_{b_{s^2}, \delta}(k) + b_{3\text{nl}} \sigma_3^2(k) P(k), \end{aligned} \quad (12)$$

where we redefine the bias parameters as

$$b_1 = c_\delta + \frac{34}{21} c_{\delta^2} \sigma^2 + \frac{1}{2} c_{\delta^3} \sigma^2 + \frac{1}{3} c_{\delta s^2} \sigma^2 + \frac{1}{2} c_{\delta e^2} \sigma_e^2 + \frac{68}{63} c_{s^2} \sigma^2 - \frac{16}{63} c_{st} \sigma^2, \quad (13)$$

$$b_2 = c_{\delta^2}, \quad (14)$$

$$b_{s^2} = c_{s^2}, \quad (15)$$

$$b_{3\text{nl}} = -\frac{16}{21} c_{s^2} + \frac{32}{105} c_{st} + \frac{512}{2205} c_\psi, \quad (16)$$

and terms associated with these bias parameters are defined as

$$P_{b_2, \delta}(k) \equiv \int \frac{d^3 q}{(2\pi)^3} P(q) P(|\mathbf{k}-\mathbf{q}|) F_S^{(2)}(\mathbf{q}, \mathbf{k}-\mathbf{q}), \quad (17)$$

$$\begin{aligned} P_{b_{s^2}, \delta}(k) &\equiv \int \frac{d^3 q}{(2\pi)^3} P(q) P(|\mathbf{k}-\mathbf{q}|) F_S^{(2)}(\mathbf{q}, \mathbf{k}-\mathbf{q}) \\ &\quad \times S^{(2)}(\mathbf{q}, \mathbf{k}-\mathbf{q}). \end{aligned} \quad (18)$$

Thus all the third-order nonlocal bias terms can be grouped into only one bias parameter, $b_{3\text{nl}}$. The main purpose of this paper is to investigate whether the $b_{3\text{nl}}$ term is important to explain the halo-matter power spectrum in N -body simulations.

B. The cross power spectrum between halo density and matter momentum

Let us next extend to the case of the cross spectrum between halo density and matter momentum. Higher-order nonlocal bias could also affect the cross spectrum between halo density and matter momentum. An advantage of the momentum spectrum is that it can be easily measured from N -body simulations without any ambiguity in interpolating the velocity divergence field [66]. Also, since the momentum spectrum is an essential ingredient in predicting the nonlinear RSDs (see [64–69]), it would be important to see an impact of the nonlocal bias terms on the momentum spectrum. Here we derive an explicit formula including the nonlocal bias terms up to third order and show that it can be renormalized in a similar manner to the case of halo and matter density correlation.

The cross spectrum between halo density and matter momentum, $P_{01}^{\text{hm}}(k)$ is given by

$$\begin{aligned} P_{01}^{\text{hm}}(\mathbf{k}) &(2\pi)^3 \delta_D(\mathbf{k} + \mathbf{k}') \\ &= \langle T_{\parallel}^{\text{h},0}(\mathbf{k}) T_{\parallel}^{\text{m},1}(\mathbf{k}') \rangle \\ &= if \frac{\mu}{k} \langle \delta_{\text{h}}(\mathbf{k}) \theta(\mathbf{k}') \rangle \\ &\quad + if \int \frac{d^3 q}{(2\pi)^3} \frac{q_{\parallel}}{q^2} \langle \delta_{\text{h}}(\mathbf{k}) \theta(-\mathbf{q}) \delta(\mathbf{k}' + \mathbf{q}) \rangle, \end{aligned} \quad (19)$$

where f is the growth parameter defined by $f \equiv d \ln D / d \ln a$ with D and a being the linear growth rate and scale factor of the Universe, respectively, and μ is cosine of the

angle between wave vector and line of sight. We define an isotropic part, $P_{01}^{\text{hm}}(k)$, as $P_{01}^{\text{hm}}(\mathbf{k}) = i\mu P_{01}^{\text{hm}}(k)/k$, motivated by the fact that it reduces to

$$P_{01}^{\text{hm}}(\mathbf{k}) = i\frac{\mu}{k}c_{\delta}fP(k), \quad (20)$$

in linear regime. The bispectrum term in Eq. (19) is not affected by the third-order perturbations, while the first term in Eq. (19) is. We then redo the similar renormalization procedure in the first term, i.e., the cross spectrum between halo density and matter velocity fields which becomes

$$\begin{aligned} P_{\delta_h\theta}(k) &= c_{\delta}P(k) + c_{\delta}P_{\delta\theta}^{(13)}(k) + c_{\delta}P_{\delta\theta}^{(22)}(k) + \frac{34}{21}c_{\delta^2}\sigma^2P(k) + \frac{1}{2}c_{\delta^3}\sigma^2P(k) + \frac{1}{3}c_{\delta s^2}\sigma^2P(k) + \frac{1}{2}c_{\delta e^2}\sigma_e^2P(k) \\ &+ c_{\delta^2}\int\frac{d^3q}{(2\pi)^3}P(q)P(|\mathbf{k}-\mathbf{q}|)G_S^{(2)}(\mathbf{q},\mathbf{k}-\mathbf{q}) + c_{s^2}\int\frac{d^3q}{(2\pi)^3}P(q)P(|\mathbf{k}-\mathbf{q}|)G_S^{(2)}(\mathbf{q},\mathbf{k}-\mathbf{q})S^{(2)}(\mathbf{q},\mathbf{k}-\mathbf{q}) \\ &+ 2c_{s^2}P(k)\int\frac{d^3q}{(2\pi)^3}P(q)F_S^{(2)}(-\mathbf{q},\mathbf{k})S^{(2)}(\mathbf{q},\mathbf{k}-\mathbf{q}) + 2c_{s^2}P(k)\int\frac{d^3q}{(2\pi)^3}P(q)D_S^{(2)}(-\mathbf{q},\mathbf{k})S^{(2)}(\mathbf{q},\mathbf{k}-\mathbf{q}) \\ &+ 2c_{\psi}P(k)\int\frac{d^3q}{(2\pi)^3}P(q)\left[\frac{3}{2}D_S^{(3)}(\mathbf{q},-\mathbf{q},-\mathbf{k}) - 2F_S^{(2)}(-\mathbf{q},\mathbf{k})D_S^{(2)}(\mathbf{q},\mathbf{k}-\mathbf{q})\right]. \end{aligned} \quad (21)$$

Since the last three lines are exactly same with the terms in the halo-density and matter-density spectrum, we confirm that $P_{\delta_h\theta}(k)$ can be similarly renormalized as

$$\begin{aligned} P_{\delta_h\theta}(k) &= b_1P_{\delta\theta}^{\text{NL}}(k) + b_2P_{b2,\theta}(k) + b_{s^2}P_{bs2,\theta}(k) \\ &+ b_{3\text{nl}}\sigma_3^2(k)P(k), \end{aligned} \quad (22)$$

where we define the terms associated with the second-order bias as

$$P_{b2,\theta}(k) \equiv \int\frac{d^3q}{(2\pi)^3}P(q)P(|\mathbf{k}-\mathbf{q}|)G_S^{(2)}(\mathbf{q},\mathbf{k}-\mathbf{q}), \quad (23)$$

$$\begin{aligned} P_{bs2,\theta}(k) &\equiv \int\frac{d^3q}{(2\pi)^3}P(q)P(|\mathbf{k}-\mathbf{q}|)G_S^{(2)}(\mathbf{q},\mathbf{k}-\mathbf{q}) \\ &\times S^{(2)}(\mathbf{q},\mathbf{k}-\mathbf{q}). \end{aligned} \quad (24)$$

A symmetric structure in integrations of the bispectrum allows us to write down the second term in Eq. (19) as [70,71]:

$$\begin{aligned} &\int\frac{d^3q}{(2\pi)^3}\frac{q_{\parallel}}{q^2}\langle\delta_h(\mathbf{k})\theta(-\mathbf{q})\delta(\mathbf{k}'+\mathbf{q})\rangle \\ &= \frac{\mu}{k}\{c_{\delta}B_{b1}(k) + c_{\delta^2}B_{b2}(k) + c_{s^2}B_{bs2}(k)\} \\ &\times (2\pi)^3\delta_D(\mathbf{k}+\mathbf{k}') \end{aligned} \quad (25)$$

$$\begin{aligned} &\simeq \frac{\mu}{k}\{b_1B_{b1}(k) + b_2B_{b2}(k) + b_{s^2}B_{bs2}(k)\} \\ &\times (2\pi)^3\delta_D(\mathbf{k}+\mathbf{k}'), \end{aligned} \quad (26)$$

where $B_{b1}(k)$, $B_{b2}(k)$ and $B_{bs2}(k)$ are expressed as follows:

$$\begin{aligned} \frac{\mu}{k}B_{b1}(k) &\equiv \int\frac{d^3q}{(2\pi)^3}\frac{q_{\parallel}}{q^2}2\{P(q)P(|\mathbf{k}-\mathbf{q}|)F_S^{(2)}(\mathbf{q},\mathbf{k}-\mathbf{q}) \\ &+ P(q)P(k)F_S^{(2)}(\mathbf{q},-\mathbf{k}) + P(|\mathbf{k}-\mathbf{q}|)P(k) \\ &\times G_S^{(2)}(\mathbf{k}-\mathbf{q},-\mathbf{k})\}, \end{aligned} \quad (27)$$

$$\frac{\mu}{k}B_{b2}(k) \equiv \int\frac{d^3q}{(2\pi)^3}\frac{q_{\parallel}}{q^2}P(q)P(|\mathbf{k}-\mathbf{q}|), \quad (28)$$

$$\frac{\mu}{k}B_{bs2}(k) \equiv \int\frac{d^3q}{(2\pi)^3}\frac{q_{\parallel}}{q^2}P(q)P(|\mathbf{k}-\mathbf{q}|)S^{(2)}(\mathbf{q},\mathbf{k}-\mathbf{q}). \quad (29)$$

Collecting all the terms in Eqs. (22) and (26), we finally obtain

$$\begin{aligned} P_{01}^{\text{hm}}(k) &= b_1\{P_{\delta\theta}^{\text{NL}}(k) + B_{b1}(k)\} + b_2\{P_{b2,\theta}(k) + B_{b2}(k)\} \\ &+ b_{s^2}\{P_{bs2,\theta}(k) + B_{bs2}(k)\} + b_{3\text{nl}}\sigma_3^2(k)P(k). \end{aligned} \quad (30)$$

Thus the cross spectrum between halo density and matter momentum also includes only the $b_{3\text{nl}}$ term as a third-order nonlocal bias. Note that the first bracket, $\{P_{\delta\theta}^{\text{NL}} + B_{b1}(k)\}$, is nothing but the cross spectrum between matter density and momentum, $P_{01}^{\text{mm}}(k)$, which is easily measured from simulations.

In summary, we show that we only need four physical and renormalized bias parameters to describe the halo-matter spectra; the renormalized linear bias parameter, b_1 , the second-order local bias parameter, b_2 , the second-order nonlocal bias parameter, b_{s^2} , and the third-order nonlocal bias parameter, $b_{3\text{nl}}$. We show the shape of each terms

discussed so far in Fig. 1, together with the nonlinear matter power spectra in our simulations. Each line corresponds to the case in which the bias parameter is equal to be unity. As shown in the figures, the third-order nonlocal bias terms can dominate over the second-order local and nonlocal terms. As we will confirm later, the third-order nonlocal bias term becomes more significant than the second-order terms especially as long as the b_2 term is sufficiently small. This is not the case at massive halos with $M_{\text{halo}} \gtrsim 5 \times 10^{13} [M_{\odot}/h]$ where b_2 becomes large enough to dominate over the $b_{3\text{nl}}$ term.

C. The bispectrum and the bias renormalization

So far we have observed that the four bias parameters, i.e., $(b_1, b_2, b_{s^2}, b_{3\text{nl}})$ are introduced to describe the cross power spectrum between halo density and matter density, or the one between halo density and matter momentum at the next-to-leading order when the nonlocal bias terms are considered. As is discussed in Ref. [53], the bispectrum at the lowest order (i.e., at tree level) demands perturbations only up to the second order, described as

$$B_{000}^{\text{hmm}}(\mathbf{k}_1, \mathbf{k}_2, \mathbf{k}_3) = b_1 B_{000}^{\text{mmm}}(\mathbf{k}_1, \mathbf{k}_2, \mathbf{k}_3) + P(k_1)P(k_2) \left[b_2 + b_{s^2} \left(\mu_{k_1, k_2}^2 - \frac{1}{3} \right) \right], \quad (31)$$

where μ_{k_1, k_2} is cosine of the angle between \mathbf{k}_1 and \mathbf{k}_2 , and the three arguments satisfy $\mathbf{k}_1 + \mathbf{k}_2 + \mathbf{k}_3 = 0$. In order to derive this as well as Eq. (26) starting from Eq. (A10), one may notice that a nontrivial approximation has been introduced, namely, $b_1 \simeq c_1$. However, Ref. [55] argued that this is not the case. As we have seen in the renormalization procedure, all the renormalized terms originate from those in the limit of $k \rightarrow 0$. This fact means that a *physical* biased field should be defined so

that homogeneous mean density is recovered at $k \rightarrow 0$. In other words, we should start with

$$\delta_{\text{h}}(\mathbf{x}) = b_1 \delta_{\text{m}}(\mathbf{x}) + \frac{1}{2} b_2 [\delta_{\text{m}}(\mathbf{x})^2 - \langle \delta_{\text{m}}(\mathbf{x})^2 \rangle] + \frac{1}{2} b_{s^2} [s(\mathbf{x})^2 - \langle s(\mathbf{x})^2 \rangle] + \dots, \quad (32)$$

rather than Eq. (A10), and hence Eqs. (26) and (31) are naturally derived. The same argument can be found in [56] as well.

Reference [53] shows that the specific μ_{k_1, k_2} dependence in Eq. (31) enables us to reliably determine both of the second-order bias parameters, b_2 and b_{s^2} at the same time from the large-scale bispectrum. In later section we are going to simultaneously fit the power spectrum as well as the bispectrum, while Ref. [53] fit the bispectrum with a prior on the linear bias b_1 determined from the halo-matter power spectrum only at $z = 0$. In Appendix B, we present the results when we fit solely to the bispectrum with b_1 treated as free. In short, the differences in two approaches are generally small especially for b_{s^2} , indicating that b_{s^2} is essentially determined by the characteristic μ_{k_1, k_2} dependence.

D. Coevolution of halos and dark matter up to third order

So far we have discussed what kind of nonlocal bias terms are allowed in terms of symmetry in the fields set by gravity. Another way of studying the nonlocal bias terms induced by nonlinear gravitational evolution is to perturbatively solve the coupled equations between halos and dark matter under fluid approximation. This coevolution picture was first introduced by [72], followed by e.g., [53, 54, 73, 74]. Here we simply assume the initial condition is purely local in the Lagrangian space, and thus this simple coevolution approach corresponds to the local Lagrangian

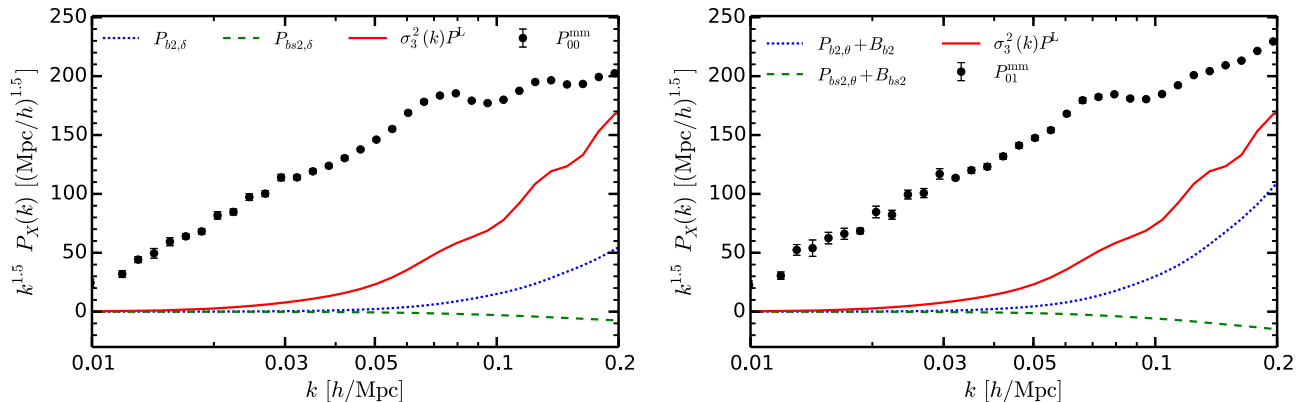


FIG. 1 (color online). A comparison of the PT correction terms at $z = 0$ for P_{00}^{hm} (left) and P_{01}^{hm} (right). The data points are the nonlinear matter power spectrum directly measured from our simulations described in Sec. III.

evolution model. Assuming no velocity bias and a conservation of halo number, the continuity and the Euler equations combined with the Poisson equation for a matter-halo system are given by

$$\delta_h(\mathbf{k}, y)' - \theta(\mathbf{k}, y) = \int \frac{d^3 q}{(2\pi)^3} \alpha(\mathbf{q}, \mathbf{k} - \mathbf{q}) \theta(\mathbf{q}, y) \delta_h(\mathbf{k} - \mathbf{q}, y), \quad (33)$$

$$\delta_m(\mathbf{k}, y)' - \theta(\mathbf{k}, y) = \int \frac{d^3 q}{(2\pi)^3} \alpha(\mathbf{q}, \mathbf{k} - \mathbf{q}) \theta(\mathbf{q}, y) \delta_m(\mathbf{k} - \mathbf{q}, y), \quad (34)$$

$$\begin{aligned} \{f\theta(\mathbf{k}, \eta)\}' + \left(1 + \frac{\mathcal{H}'}{\mathcal{H}^2}\right) \theta(\mathbf{k}, y) - \frac{3}{2f} \Omega_m(y) \delta_m(\mathbf{k}, y) \\ = f \int \frac{d^3 q}{(2\pi)^3} \beta(\mathbf{q}, \mathbf{k} - \mathbf{q}) \theta(\mathbf{q}, \eta) \theta(\mathbf{k} - \mathbf{q}, \eta), \end{aligned} \quad (35)$$

where we introduce $y \equiv \ln D(\eta)$ as a time variable rather than the conformal time η , and the prime denotes derivative w.r.t y . The Hubble parameter \mathcal{H} is defined by $\mathcal{H} = da/(ad\eta)$. The linear-order solutions for this system are given by $\delta_m^{(1)}(\mathbf{k}, y) = e^y \delta_0(\mathbf{k}, y_i)$, $\theta^{(1)}(\mathbf{k}, y) = \delta^{(1)}(\mathbf{k}, y)$, and $\delta_h^{(1)}(\mathbf{k}, y) = b_1^E(y) e^y \delta_0(\mathbf{k}, y_i)$ where

$$\frac{b_1^L(y)}{b_1^L(y_i)} = \frac{b_1^E(y) - 1}{b_1^E(y_i) - 1} = \frac{e^{y_i}}{e^y}. \quad (36)$$

As is shown in Ref. [53,54,75], the second-order solution for halos is written by

$$\begin{aligned} \delta_h^{(2)}(\mathbf{k}, y) = b_1^E(y) \int \frac{d^3 q}{(2\pi)^3} F_S^{(2)}(\mathbf{q}, \mathbf{k} - \mathbf{q}) \delta_m^{(1)}(\mathbf{q}, y) \\ \times \delta_m^{(1)}(\mathbf{k} - \mathbf{q}, y) + \left\{ \frac{1}{2} b_2^L(y) + \frac{4}{21} b_1^L(y) \right\} \\ \times \int \frac{d^3 q}{(2\pi)^3} \delta_m^{(1)}(\mathbf{q}, \eta) \delta_m^{(1)}(\mathbf{k} - \mathbf{q}, y) - \frac{2}{7} b_1^L(y) \\ \times \int \frac{d^3 q}{(2\pi)^3} S^{(2)}(\mathbf{q}, \mathbf{k} - \mathbf{q}) \delta_m^{(1)}(\mathbf{q}, y) \delta_m^{(1)}(\mathbf{k} - \mathbf{q}, y), \end{aligned} \quad (37)$$

where we used the fact that $b_n^L(y) = b_n^L(y_i) e^{n(y-y_i)}$. Hence a correspondence of the local and nonlocal bias terms at second order to Eq. (A14) is clearly found, and it shows that the tidal field is allowed to be a source of the nonlocal bias at second order:

$$b_2^{\text{coev}} = b_2^L(y) + \frac{8}{21} b_1^L(y), \quad (38)$$

$$b_{s^2}^{\text{coev}} = -\frac{4}{7} b_1^L(y) = -\frac{4}{7} (b_1^E(y) - 1). \quad (39)$$

Continuing to this exercise to third order, we find the solution as

$$\begin{aligned} \delta_h^{(3)}(\mathbf{k}, y) = \delta_h^{(3)}(\mathbf{k}, y_i) + \frac{1}{3} \int \frac{d^3 q_1}{(2\pi)^3} \frac{d^3 q_2}{(2\pi)^3} G_S^{(3)}(\mathbf{q}_1, \mathbf{q}_2, \mathbf{k} - \mathbf{q}_1 - \mathbf{q}_2) \delta_m^{(1)}(\mathbf{q}_1, y) \delta_m^{(1)}(\mathbf{q}_2, y) \delta_m^{(1)}(\mathbf{k} - \mathbf{q}_1 - \mathbf{q}_2, y) \\ + \left(\frac{1}{2} b_1^L(y) + \frac{1}{3} \right) \int \frac{d^3 q_1}{(2\pi)^3} \frac{d^3 q_2}{(2\pi)^3} [\alpha(\mathbf{q}_1, \mathbf{q}_2 + \mathbf{q}_3) F_S^{(2)}(\mathbf{q}_2, \mathbf{q}_3)]_{\text{sym}} \delta^3 \\ + \left[\frac{1}{2} b_2^L(y) + \frac{2}{21} b_1^L(y) \right] \int \frac{d^3 q_1}{(2\pi)^3} \frac{d^3 q_2}{(2\pi)^3} [\alpha(\mathbf{q}_1, \mathbf{q}_2 + \mathbf{q}_3)]_{\text{sym}} \delta^3 \\ - \frac{1}{4} b_{s^2} \int \frac{d^3 q_1}{(2\pi)^3} \frac{d^3 q_2}{(2\pi)^3} [\alpha(\mathbf{q}_1, \mathbf{q}_2 + \mathbf{q}_3) S^{(2)}(\mathbf{q}_2, \mathbf{q}_3)]_{\text{sym}} \delta^3 \\ + \left(\frac{1}{2} b_1^L(y) + \frac{1}{3} \right) \int \frac{d^3 q_1}{(2\pi)^3} \frac{d^3 q_2}{(2\pi)^3} [\alpha(\mathbf{q}_2 + \mathbf{q}_3, \mathbf{q}_1) G_S^{(2)}(\mathbf{q}_2, \mathbf{q}_3)]_{\text{sym}} \delta^3. \end{aligned} \quad (40)$$

Although the third-order solution looks somewhat complicated, it is useful to isolate its contribution to the matter-halo power spectrum, i.e., $\langle \delta_h^{(3)}(\mathbf{k}, y) \delta_m^{(1)}(\mathbf{k}, y) \rangle$. Subtracting out the terms proportional to the linear bias, we find

$$P_{\text{coev}}^{\text{hm},(31)}(k) - b_1^E P^{(31)}(k) = \frac{32}{315} b_1^L \sigma_3^2 P(k) + \left(b_2^L + \frac{1}{2} b_3^L \right) \sigma^2 P(k). \quad (41)$$

Now it is straightforward to correspond this formula to Eq. (12):

$$b_{3\text{nl}}^{\text{coev}} = \frac{32}{315} b_1^L(y) = \frac{32}{315} (b_1^E(y) - 1), \quad (42)$$

$$b_1 = b_1^E + \left(b_2^L + \frac{1}{2} b_3^L \right) \sigma^2. \quad (43)$$

Thus the nonlocal bias term at third order which we discussed in the previous section can be related to the linear Lagrangian bias in this specific way. We will compare this prediction with our $b_{3\text{nl}}$ measurement from simulations in the following sections.

III. N -BODY SIMULATIONS AND THE FITTING METHODOLOGY

A. N -body simulation detail

We performed a suite of N -body simulations using the publicly available GADGET2 code [76] to make 14 realizations at $z = 0, 0.5$ and 1 with cosmological parameters in a flat Λ CDM model preferred by the WMAP results [1], i.e., a mass density parameter $\Omega_m = 0.272$, a baryon density parameter $\Omega_b = 0.0455$, a Hubble constant $h = 0.704$, a spectral index $n_s = 0.967$, and a normalization of the curvature perturbations of $\Delta_{\mathcal{R}}^2 = 2.42 \times 10^{-9}$ at the pivot scale of $k = 0.002 \text{ Mpc}^{-1}$, giving $\sigma_8 = 0.81$. The total simulation volume is $47.25[(\text{Gpc}/h)^3]$ which is larger roughly by a factor of ten than the current galaxy survey like BOSS. We generated initial conditions at $z = 99$ using the second-order Lagrangian perturbation theory to initialize the second order growth correctly and allow for a reliable bispectrum extraction at low redshift. The box size and number of particles are $L = 1500 \text{ Mpc}/h$ and $N_{\text{particle}} = 1024^3$, respectively, yielding a particle mass resolution of $2.37 \times 10^{11} M_{\odot}/h$.

We identify halos using the Friends-of-Friends finder with a linking length of 0.2 times the mean inter particle spacing. We only take halos which contain more than 20 particles, and hence our minimum halo mass is approximately $4.74 \times 10^{12} M_{\odot}/h$. We divide the halo catalog into several mass bins at each redshift slice, whose detail is summarized in Table I. Note that $\sim 10^{13} M_{\odot}/h$ halo roughly corresponds to a typical host halo in which observed galaxies live. In order to estimate the power spectrum and the bispectrum, the

particles are assigned on a $N_c = 1024$ grid with the Cloud-in-Cell algorithm, and the gridded density field is properly corrected by the window function. We also estimate the power spectrum of mass-weighted momentum of matter, following the method in [65,66]. Note that our simulation is different from that used in [53,65,66,77]. We mainly focus on combined measurement using the power spectrum and the bispectrum but will present results in the case of the bispectrum only in Appendix B.

The errors of the power spectrum are estimated by the standard deviation among 14 realizations. Strictly speaking, it might be necessary to evaluate the covariance matrix to take account for the off-diagonal correlation among different modes. However, we neglect the correlation between different modes, since we focus on somewhat large scales, $k \lesssim 0.1h/\text{Mpc}$. This part can be definitely improved by a proper treatment of the covariance matrix with larger number of realizations.

B. Fitting procedure

Let us briefly summarize how we determine the bias parameters from the simulated power spectra. As explained in the previous section, we have four bias parameters as free, i.e., two local bias parameters, b_1 and b_2 , and second- and third-order nonlocal bias ones, b_{s^2} and $b_{3\text{nl}}$. When we fit the bias model to the halo-matter density power spectrum only, the fitted bias parameters are estimated so that they minimize

$$\chi_{P_{00}}^2 = \sum_{k_i \leq k_{\text{max},P(k)}} \frac{[P_{00}^{\text{hm}}(k_i) - \hat{P}_{00}^{\text{hm}}(k_i)]^2}{\Delta P_{00}^{\text{hm}}(k_i)^2}. \quad (44)$$

Here theoretical template of P_{00}^{hm} at $k = k_i$ is given by Eq. (12), \hat{P}_{00}^{hm} denotes the spectrum measured from the simulations, $\Delta P_{00}^{\text{hm}}$ denotes the error of the spectrum amplitude, and $k_{\text{max},P(k)}$ is the maximum wave number in

TABLE I. Summary of halo catalogs used in this paper. We also show the best-fitting values of four bias parameters determined by our fitting from the power spectrum and the bispectrum. The fitting range, k_{max} , depends on redshift (see text on how to choose k_{max} in detail): $(k_{\text{max},P(k)}, k_{\text{max},B(k)}) = (0.08, 0.065)$, $(0.10, 0.075)$, and $(0.125, 0.075)$ at $z = 0, 0.5$ and 1, respectively. Note that the definition of second-order bias parameters in [53] differs by a factor of two.

| Redshift | Mass bin | $\bar{M}_{\text{halo}} [10^{13} M_{\odot}/h]$ | b_1 | b_2 | b_{s^2} | $b_{3\text{nl}}$ |
|----------|----------|---|---------------------|--------------------|--------------------|--------------------|
| 1 | I | 0.763 | 2.0419 ± 0.0089 | -0.168 ± 0.027 | -1.099 ± 0.064 | 0.211 ± 0.074 |
| | II | 2.24 | 2.7957 ± 0.0114 | 1.766 ± 0.039 | -1.409 ± 0.094 | 0.133 ± 0.100 |
| | III | 6.50 | 4.0294 ± 0.0170 | 8.0362 ± 0.062 | -1.708 ± 0.165 | 0.245 ± 0.150 |
| 0.5 | I | 0.769 | 1.4426 ± 0.0057 | -0.792 ± 0.018 | -0.469 ± 0.038 | 0.153 ± 0.030 |
| | II | 2.29 | 1.9033 ± 0.0078 | -0.394 ± 0.024 | -0.785 ± 0.052 | 0.170 ± 0.043 |
| | III | 6.75 | 2.7005 ± 0.0115 | 1.586 ± 0.035 | -1.286 ± 0.080 | 0.268 ± 0.061 |
| | IV | 19.3 | 4.1349 ± 0.0204 | 8.650 ± 0.066 | -1.837 ± 0.155 | -0.294 ± 0.112 |
| 0 | I | 0.773 | 1.0488 ± 0.0048 | -0.777 ± 0.013 | -0.099 ± 0.026 | 0.092 ± 0.019 |
| | II | 2.33 | 1.3094 ± 0.0062 | -0.873 ± 0.018 | -0.267 ± 0.035 | 0.132 ± 0.023 |
| | III | 6.92 | 1.7977 ± 0.0087 | -0.462 ± 0.025 | -0.514 ± 0.051 | 0.193 ± 0.035 |
| | IV | 20.1 | 2.6741 ± 0.0136 | 1.500 ± 0.040 | -1.028 ± 0.086 | 0.105 ± 0.053 |

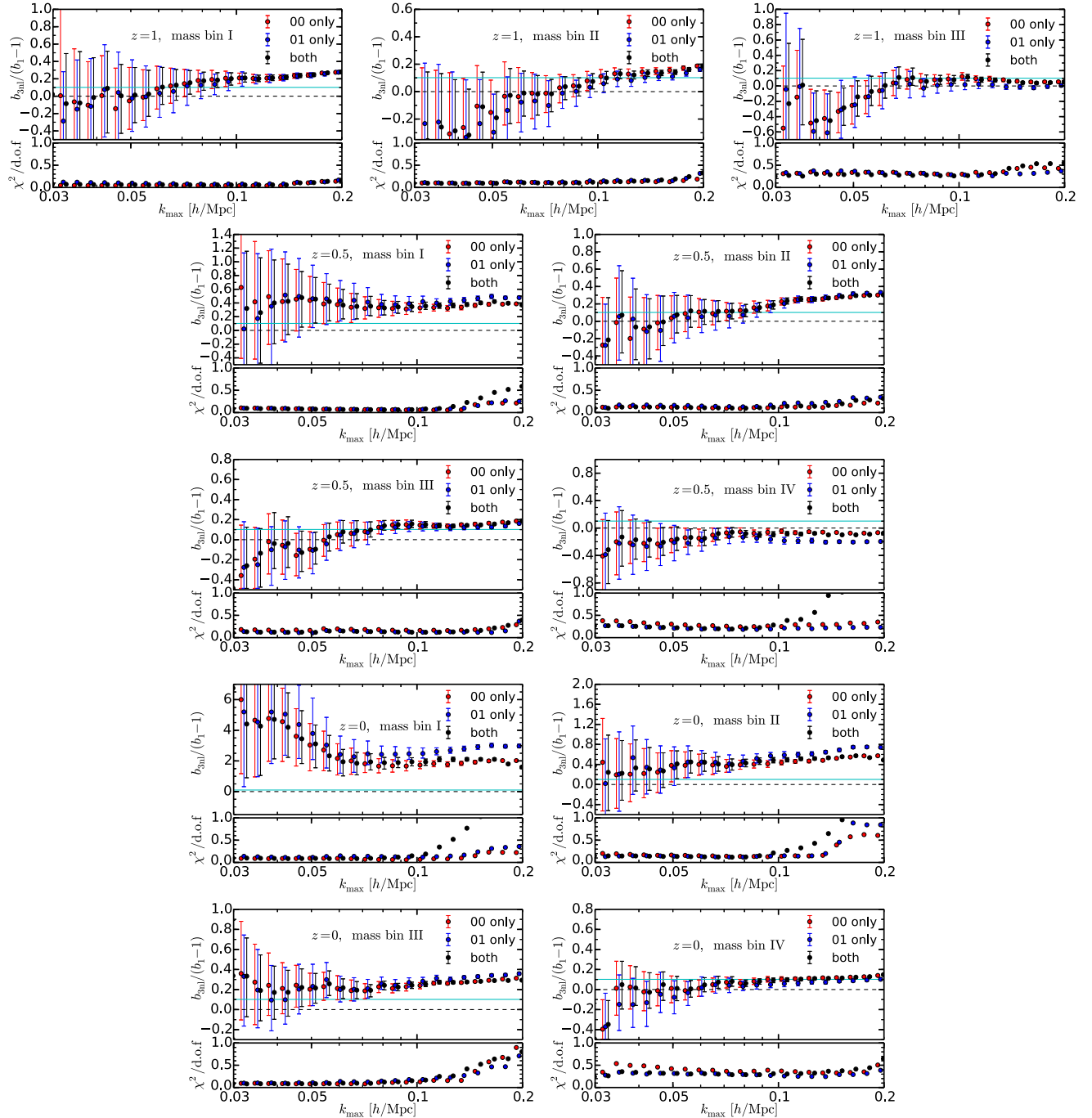


FIG. 2 (color online). The best-fitting values of b_{3nl} as a function of k_{\max} . We present results at $z = 1$ (top three), at $z = 0.5$ (middle four), and at $z = 0$ (bottom four), for light to heavy (from I to IV) halo mass bins. In each panel, we show results in the case of P_{00}^{hm} only (red), P_{01}^{hm} only (blue), and both of two (black). The goodness of fit, $\chi^2_{P(k)}/\text{dof}$, is also plotted in the lower part of each panel. Note that we jointly fit the bispectrum together with the power spectrum. For comparison, the prediction from the coevolution picture (local Lagrangian bias model), 32/315, is indicated by the horizontal line (cyan solid).

the power spectrum analysis. Likewise we apply exactly the same procedure for the cross power spectrum between halo-density and matter-momentum by replacing 00 with 01 in the subscript in Eq. (44). Note that we always insert the measured spectra from the simulation for nonlinear matter part, $P_{\delta\delta}^{\text{NL}}$ for P_{00}^{mm} and $\{P_{\delta\theta}^{\text{NL}} + B_{b1}\}$ for P_{01}^{mm} . We also note

that we use the power spectra averaged over 14 realizations rather than one in each realization. This is the reason why we will observe somewhat low values of reduced χ^2 , and hence this is not an overfitting issue. When we quote “00 only” (“01 only”), we simply use $\chi^2_{P(k)} = \chi^2_{P_{00}}$ ($\chi^2_{P(k)} = \chi^2_{P_{01}}$). When we include both P_{00}^{hm} and P_{01}^{hm} , we assume they are

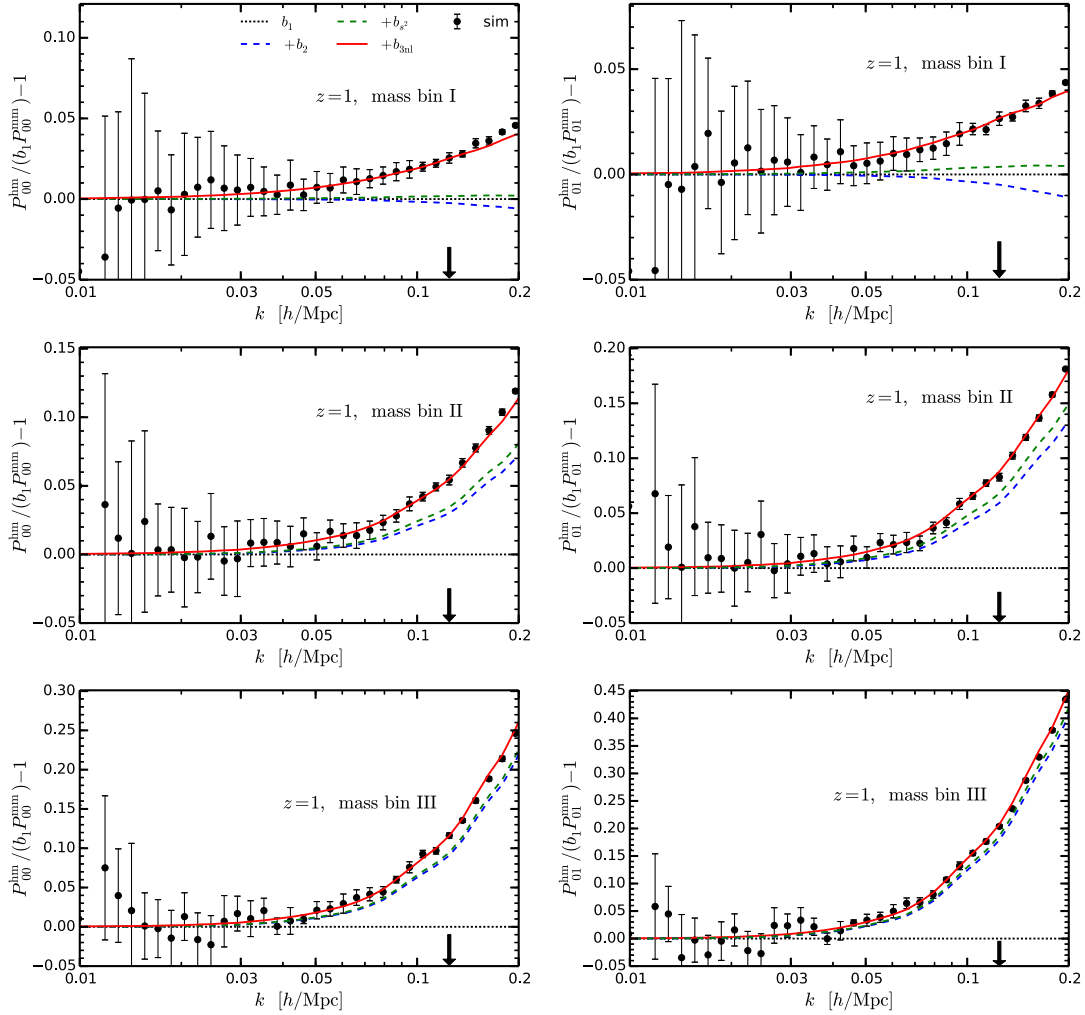


FIG. 3 (color online). The power spectra with best-fitting bias parameters at $z = 1$. We here plot $P_X^{\text{hm}}(k)/(b_1 P_X^{\text{mm}}(k)) - 1$ where X is 00 (left) or 01 (right) with the best-fitting values of b_1 and $b_{3\text{nl}}$ at $k_{\text{max}} = 0.125 h/\text{Mpc}$ (specified as an arrow). Namely, zero values (black dotted) mean it matches to the linear bias term, any deviation from zero represents deviation from the linear bias model. The red solid line corresponds to the case including all contributions. The blue dashed line includes only local bias terms up to second order, while the green dashed line includes local and nonlocal bias terms up to second order.

independent and simply add two χ^2 by neglecting the correlation between two, i.e., $\chi_{P(k)}^2 = \chi_{P00}^2 + \chi_{P01}^2$. In principle, we could estimate the covariance matrix which includes correlation between both signals but the number of our realizations would not be sufficient to properly estimate it (see e.g., [78] for a recent study in such a direction).

The similar procedure is adopted for the bispectrum as well. We search the best-fitting values of the bias parameters for the bispectrum so that they minimize

$$\chi_{B(k)}^2 = \sum_{k_{i,j} \leq k_{\text{max},B(k)}} \frac{[B_{000}^{\text{hmm}}(k_i, k_j, \mu_{ij}) - \hat{B}_{000}^{\text{hmm}}(k_i, k_j, \mu_{ij})]^2}{\Delta B_{000}^{\text{hmm}}(k_i, k_j, \mu_{ij})^2}, \quad (45)$$

where $\mu_{i,j}$ is the cosine between \mathbf{k}_1 and \mathbf{k}_2 , the theoretical template of B_{000}^{hmm} is given by Eq. (31), $\Delta B_{000}^{\text{hmm}}$ denotes the

error of the bispectrum amplitude, and $k_{\text{max},B(k)}$ is the maximum wave number in the bispectrum analysis. Notice that the bispectrum depends only on three bias parameters, b_1 , b_2 and b_{s^2} . We distinguish the maximum wave number range in the power spectrum case from that in the bispectrum. It is not entirely clear if higher-order PT terms for different statistics become dominant at the same wave number. Our main purpose is to investigate how large the third-order contribution is, and hence we fix $k_{\text{max},B(k)}$ to 0.065 ($0-075$) h/Mpc at $z = 0$ ($z = 0.5$ or 1) in the following analysis. These choices are based on our fitting results to the bispectrum only, presented in Appendix B. Thus, we adopt $\chi^2 = \chi_{P(k)}^2 + \chi_{B(k)}^2$ when we jointly fit the PT model to the power spectrum and the bispectrum.

In order to fully investigate the probability distribution of preferred values of the bias parameters, we adopt the Markov chain Monte Carlo (MCMC) technique, assuming

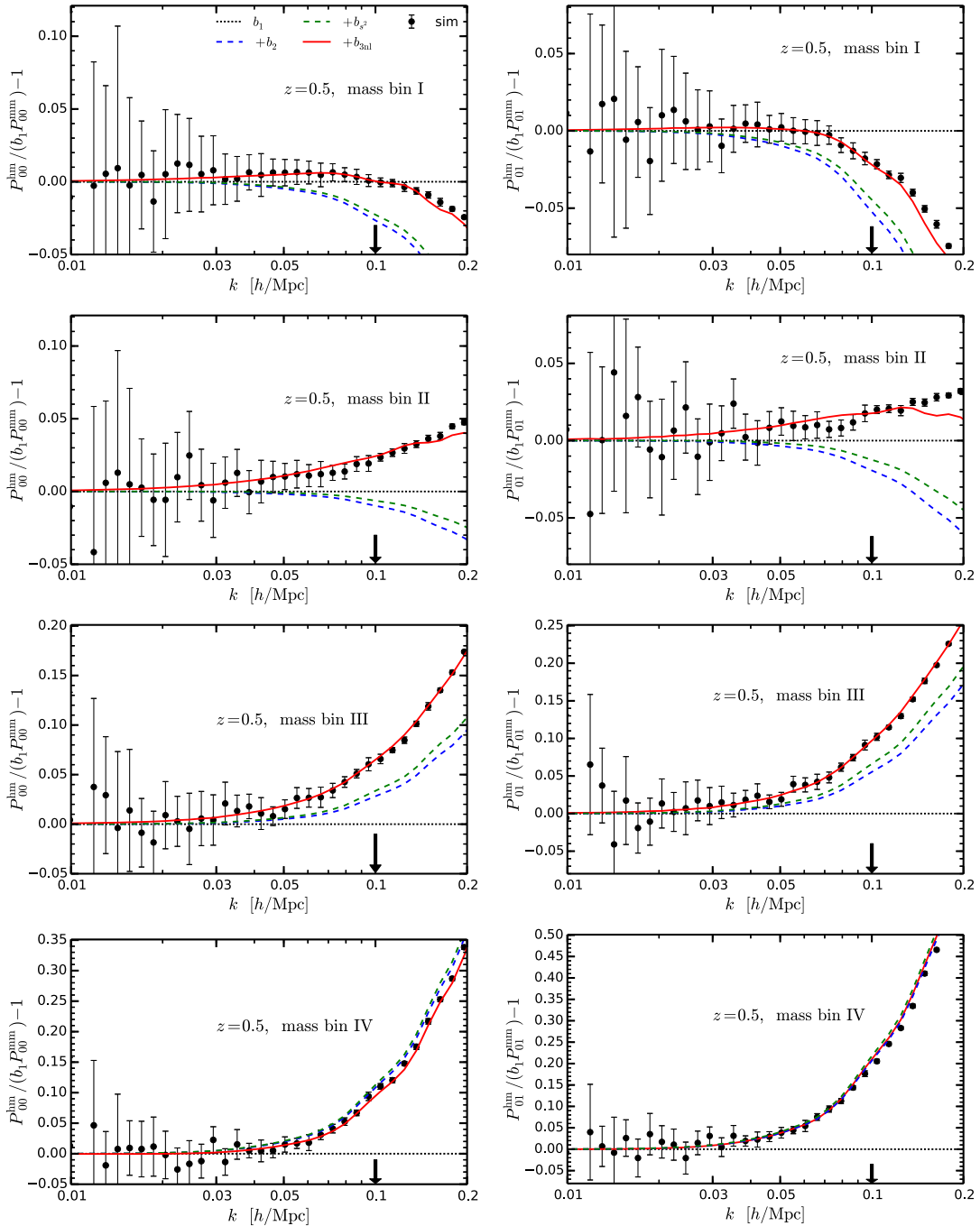


FIG. 4 (color online). Same as Fig. 3, but at $z = 0.5$. The best-fitting values are derived at $k_{\max} = 0.1 h/\text{Mpc}$ (specified as an arrow).

the Gaussian likelihood, i.e., $\mathcal{L} \propto \exp(-\chi^2/2)$. For this end, we modify the COSMOMC code [79], considering future applications of the code to the actual galaxy sample. We ensure convergence of each chain, imposing $R < 0.003$ where R is the standard Gelman-Rubin criteria.

IV. RESULTS

Now we show our measurements of the bias parameters from the simulated halo-matter power spectra combined

together with the bispectrum. In Fig. 2, we show the best-fitting values of b_{3nl} as a function of k_{\max} for each mass bin at each redshift. First of all, the preferred values of b_{3nl} are nonzero generally for any halo mass bin at any redshift, at $k_{\max} \sim 0.1 h/\text{Mpc}$. Also, the best-fitting values of b_{3nl} from $P_{00}^{\text{hm}}(k)$ are generally in a good agreement with those from $P_{01}^{\text{hm}}(k)$, indicating that the third-order nonlocal bias term is important to explain both $P_{00}^{\text{hm}}(k)$ and $P_{01}^{\text{hm}}(k)$. If looking at smaller scales at $k \gtrsim 0.1 h/\text{Mpc}$, we start to see a

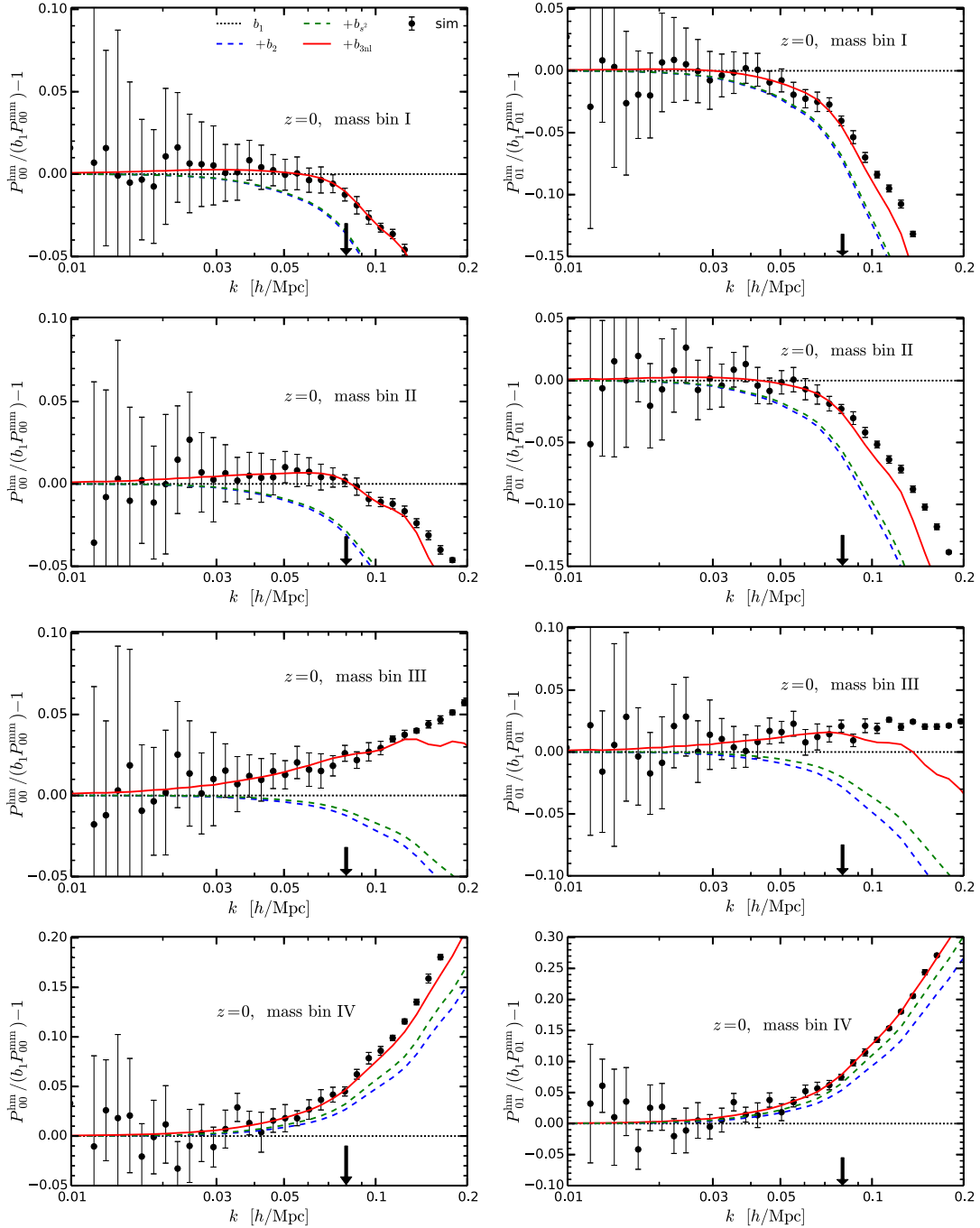


FIG. 5 (color online). Same as Fig. 3, but at $z = 0$. The best-fitting values are derived at $k_{\max} = 0.08 h/\text{Mpc}$ (specified as an arrow).

discrepancy between the two results, and the best-fitting values tend to vary as a function of k_{\max} . In addition, a goodness of fit, $\chi^2/(\text{dof})$ becomes worse at larger k . This clearly shows that our bias model fails to describe the halo-matter power spectra at such small scales, and higher-order contribution would start to kick in. Notice again that our values of the goodness of fit is somewhat small [$\mathcal{O}(0.1)$] simply because we adopt the nonlinear matter power spectra taken from the simulation itself, and we do not worry about unrealistic overfitting issues here. Since our

$b_{3\text{nl}}$ measurements look convergent up to a certain k_{\max} but start to vary at larger k_{\max} , it is difficult to define the reliable range of the bias model which could depend on both redshift and halo mass. We here simply and conservatively quote the measured values of $b_{3\text{nl}}$ at $k_{\max} = 0.08, 0.1$, and 0.125 at $z = 0, 0.5$, and 1 , respectively, which roughly correspond to valid range of the standard perturbation theory [80,81].

We quantify contribution of the third-order nonlocal bias term to each power spectrum in Figs. 3, 4, and 5 for $z = 1$,

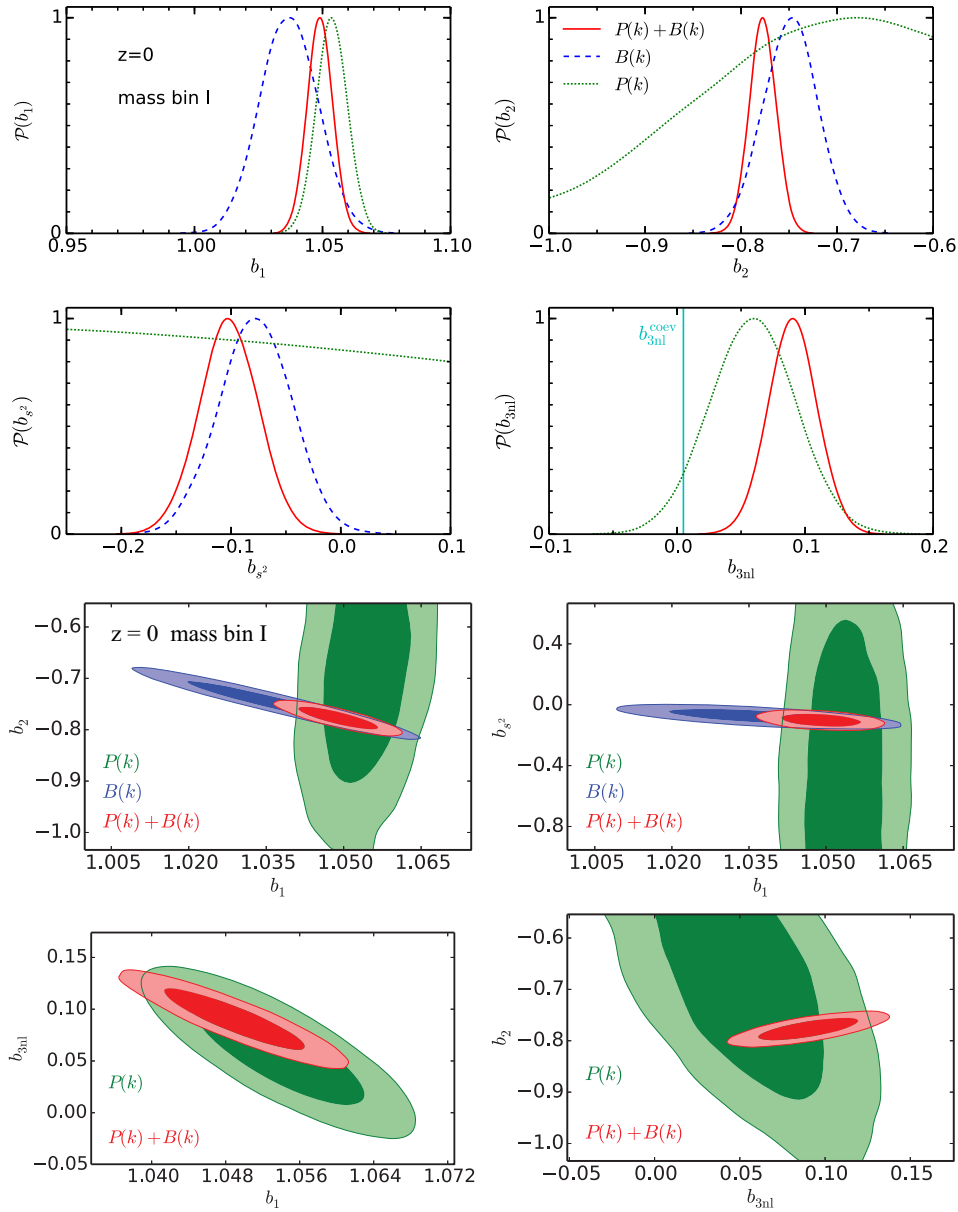


FIG. 6 (color online). (Upper four panels) comparison between cases with and without combining the bispectrum information for mass bin I at $z=0$. We show the marginalized probability distribution for each bias parameter in the cases of the power spectrum combined with the bispectrum (red solid), the bispectrum only (blue dashed), and the power spectrum only (green dotted). As a reference, we show the prediction from the coevolution b_{3nl}^{coev} assuming $b_1 \approx b_1^E$ is equal to the value obtained by joint fitting (cyan). Note that, in the case of the power spectrum, we use both density-density and density-momentum power spectrum with $k_{max,P(k)} = 0.08h/\text{Mpc}$. (Lower four panels) the marginalized two-dimensional contours (68% and 95% C.L.) among the nonlinear bias parameters.

0.5 and 0, respectively. We plot $P_X^{lm}(k)/(b_1 P_X^{mm}(k)) - 1$ with X being 00 or 01, which manifests deviation from the linear bias term. The blue lines show the nonlinear contributions from local term only, i.e., the b_2 term, while the green lines show ones from second-order local plus nonlocal terms, i.e., the b_2 term plus the b_{s^2} one. Our best-fitting results including the third-order nonlocal bias term is shown by the red curves. Clearly seen from the figures, the local bias model cannot explain the simulated

halo-matter spectra, and even including second-order nonlocal bias terms does not drastically help in general. Meanwhile, adding the third-order nonlocal bias term can apparently explain the power spectra very well. Within the valid range, the fractional differences between the simulated and fitted spectra are typically at a few percent level. This result is already expected from the behavior of the PT terms in Fig. 1. The reason why we obtain negative values of b_{3nl} at mass bin IV at $z=0.5$

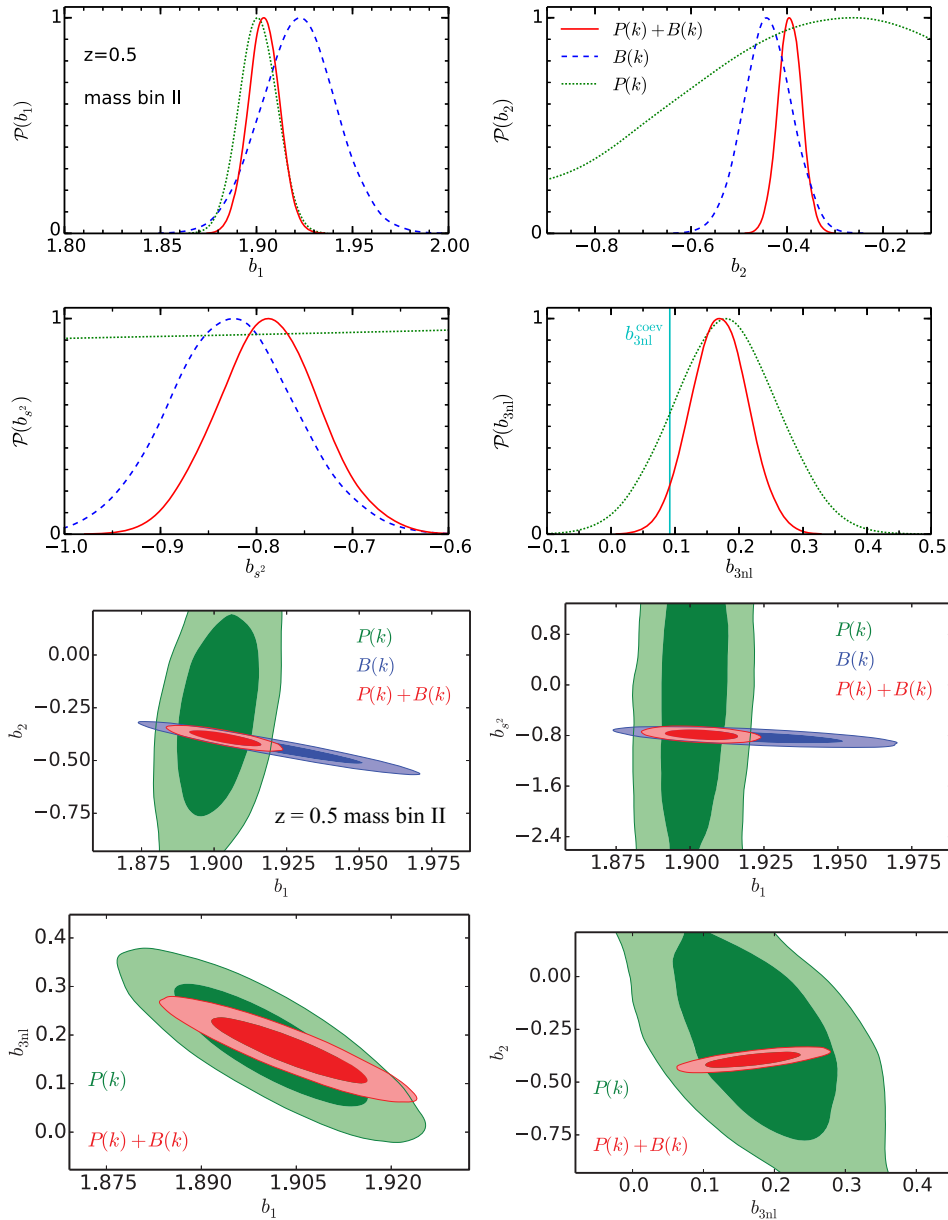


FIG. 7 (color online). Same as Fig. 6, but for mass bin II at $z = 0.5$. Note that, in the case of the power spectrum, we use both density-density and density-momentum power spectrum with $k_{\max, P(k)} = 0.1 h/\text{Mpc}$.

is obvious from the figures. At these bins, the bispectrum prefers large second-order bias parameters, especially b_2 , whose contribution exceed the measured halo-matter power spectra. Therefore the negative $b_{3\text{nl}}$ is necessary to compensate with the second-order terms.

Given the fact that the contribution of the second-order terms are generally lower than that of the third-order nonlocal term, it is interesting to see to what extent we can simultaneously constrain four bias parameters only from the power spectra, i.e., without help of information on the second-order bias parameters from the bispectrum. We often encounter a similar situation in analyzing the actual galaxy survey if we only have the power spectrum

measurement available, although we focus on the unobservable halo-matter power spectra throughout this work. Also, it is interesting to separate the information of the power spectrum out of that of the bispectrum and to understand the parameter degeneracy in the PT model. Figures 6–8 show one-dimensional and two-dimensional marginalized posterior distribution for constraints on the bias parameters. Generally speaking, the third-order nonlocal bias $b_{3\text{nl}}$ is well constrained even only from the power spectra, while the second-order bias parameters cannot be tightly constrained only by the power spectra (green). The second-order nonlocal bias, b_{s2} cannot be constrained at all by the power spectra, since the

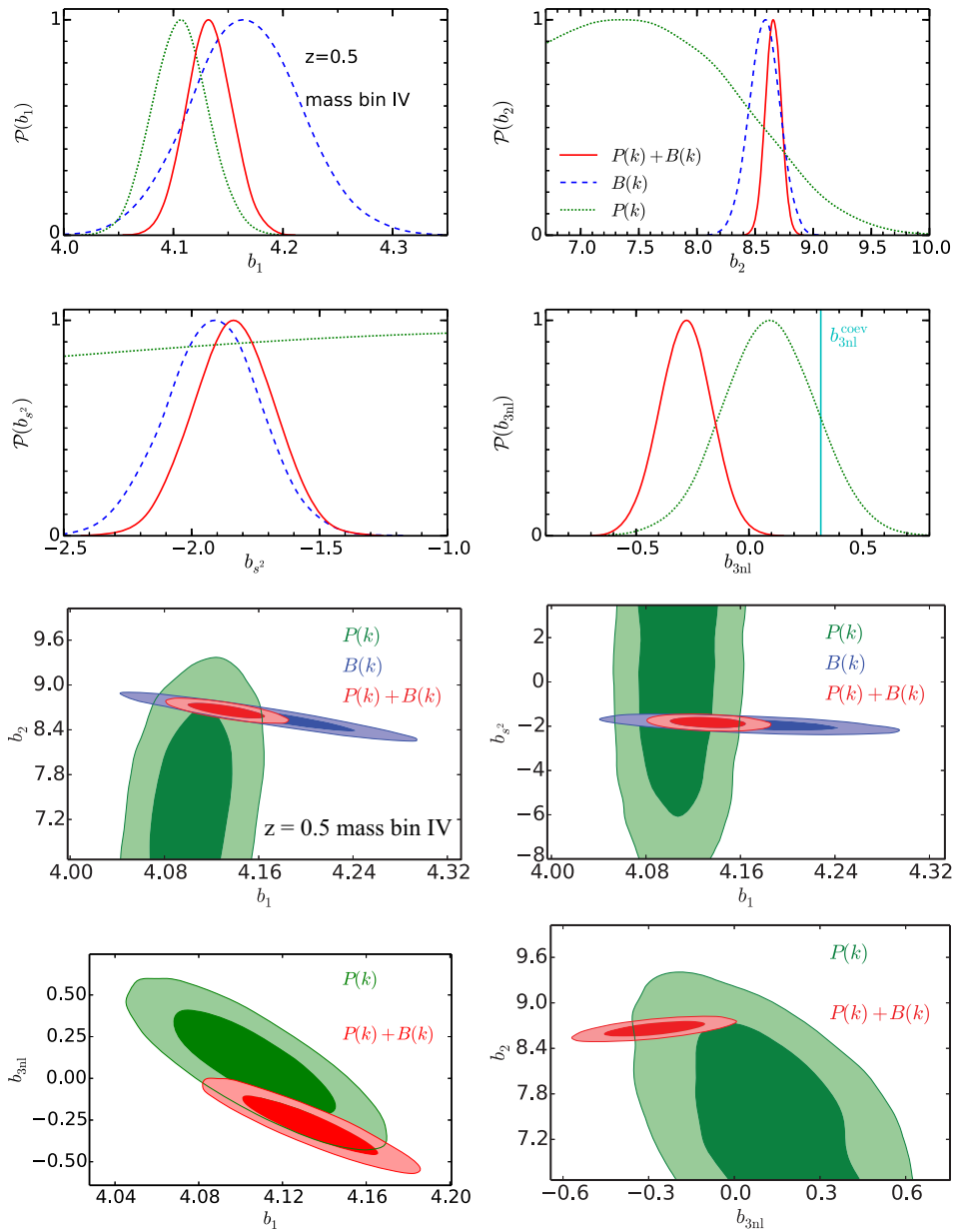


FIG. 8 (color online). Same as Fig. 6, but for mass bin IV at $z = 0.5$. Note that, in the case of the power spectrum, we use both density-density and density-momentum power spectrum with $k_{\max, P(k)} = 0.1 h/\text{Mpc}$.

amplitude of the b_{s^2} term in the power spectra is fairly small compared to other terms as seen in Fig. 1. The second-order local bias b_2 can be constrained by the power spectra, but we confirm that the bispectrum is more sensitive to b_2 . At low and intermediate mass bins (see Figs. 6 and 7), the preferred values of b_2 both from the power spectra and the bispectrum are consistent with each other, and hence the resultant values of $b_{3\text{nl}}$ in both cases of $P(k)$ and of $P(k) + B(k)$ become consistent as well. At massive bin (see Fig. 8), this story seems a bit different. Since the preferred values of b_1 and b_2 from the bispectrum at mass bin IV of $z = 0.5$ are larger than those from the power spectra, the well-fitting $b_{3\text{nl}}$ from the combined

case becomes lower than the one only from the power spectrum. Equivalently, the $b_{3\text{nl}}$ term become less important at higher mass bins, and the b_2 terms become dominant over the $b_{3\text{nl}}$ term. Furthermore, the linear bias value can be constrained solely by the bispectrum and its agreement with the power spectrum-only result becomes worse for more massive halos. The constraining power of the power spectrum on b_1 is weaker than what can be found in the literature. This is a consequence of an anticorrelation between b_1 and $b_{3\text{nl}}$. This fact implies that the $b_{3\text{nl}}$ term becomes important at fairly large scales, $k \lesssim 0.1 h/\text{Mpc}$ and has a non-negligible impact on determination of the linear bias value. We here do not investigate how

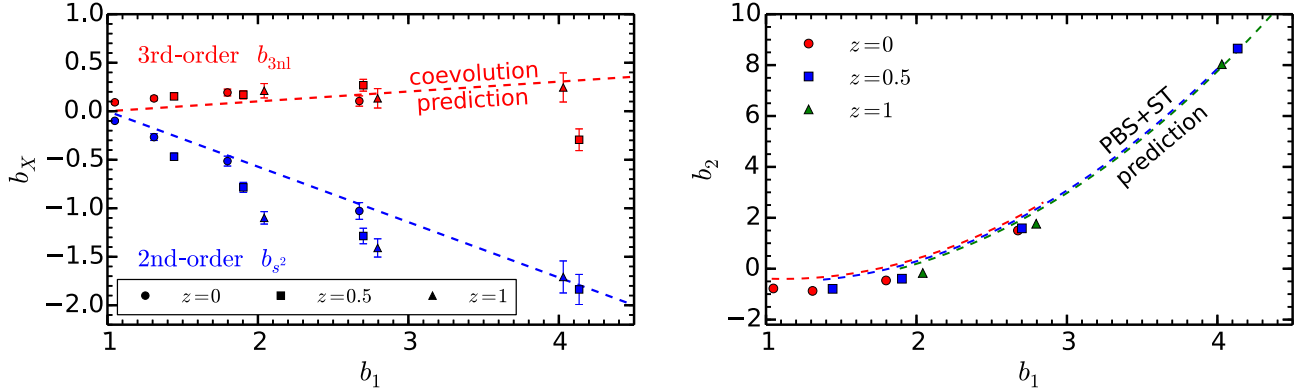


FIG. 9 (color online). (*Left*) nonlocal bias values at second and third orders as a function of the linear bias parameter. Each point is taken from the result in the joint fit of the power spectrum and the bispectrum. Both of them are compared with the values expected from the local Lagrangian bias in the simple convolution picture (*dashed* lines). (*Right*) second-order local bias b_2 against b_1 . Again each point is obtained from our joint fit. For comparison, we draw theory lines which is based on the peak-background split with the universal mass function (see text in detail). Note that the range of these lines are limited since we here consider relevant halo mass range only ($0.6 \lesssim M_{\text{halo}} [10^{13} M_{\odot}/h] \lesssim 21$).

these correlations affect estimation of cosmological parameters of interest and will be addressed in future work.

Finally, we make a comparison between our $b_{3\text{nl}}$ measurements with a theoretical prediction in order to make sure if our results are physically expected. For this purpose, we compare our results with the prediction, Eq. (42), in the simple coevolution picture (or the local Lagrangian bias) as discussed in Sec. II D. The cyan horizontal (vertical) line in each panel of Fig. 2 (Figs. 6–8) is already drawn, and the left panel of Fig. 9 summarizes such a comparison which includes both second- and third-order nonlocal bias parameters as a function of the linear bias b_1 . Notice that it is not clear if our measured b_1 truly corresponds to b_1^E [see Eq. (43)] but we here simply assume $b_1 \approx b_1^E$ for simplicity. As clearly seen in Fig. 9, overall agreement in third-order nonlocal bias is as good as that in second-order, although the agreement is apparently not perfect. Also, the $b_{3\text{nl}}$ value at mass bin IV of $z = 0.5$ exceptionally deviates from the coevolution prediction. As we discussed above, however, the value preferred from the power spectrum only is more consistent with the coevolution prediction (see green dotted line in Fig. 8). Again, this difference comes from the fact that the mass bin IV of $z = 0.5$ prefers larger b_2 which more affects the power spectrum and the bispectrum than the nonlocal bias terms. There are several sources which could make the prediction different from the local Lagrangian bias as we will discuss in the following section. However, it is worth mentioning that our $b_{3\text{nl}}$ measurement is not far from the coevolution prediction which is one of the simplest physical models one thinks of. This fact also implies an evidence of the third-order nonlocal bias term. In the right panel of Fig. 9, we also compare our measurements of the second-order local bias b_2 from the joint fit with theoretical prediction that is based on the

peak-background split (PBS) with the universal mass function (see Appendix D in detail). Clearly seen from the figure, the measured b_2 values are systematically lower than the theoretical predictions at fixed b_1 , while the characteristic dependence on b_1 is qualitatively similar. Note that it is a coincidence that two points around $b_1 \sim 4$ look in a perfect agreement with the prediction, since they deviate from predictions in (b_1, M_{halo}) or (b_2, M_{halo}) plane.

V. SUMMARY AND DISCUSSION

The nonlocality of halo bias is naturally induced by nonlinear gravitational evolution as suggested by recent studies. In this paper we study how well the PT model including nonlocal bias effects perform against the halo statistics simulated in N -body simulations in a Λ CDM universe. For this purpose we first revisit the bias renormalization scheme proposed by [51] and show that, while the leading-order bispectrum requires only one second-order nonlocal bias term, b_{s^2} [see Eq. (31)], the power spectrum at next-to-leading order demands an additional nonlocal bias term, $b_{3\text{nl}}$, associated with the third-order perturbation [see Eq. (12)]. We extend this model to the power spectrum between halo density and matter momentum, and show that there is an exactly same correction of the $b_{3\text{nl}}$ term in this case as well [see Eq. (30)]. The fact that we only need one additional nonlocal bias even at third order may sound surprising. However, we argue that this is actually expected since the symmetry in gravity basically restricts the allowed functional form of nonlocal terms. In order to confirm this, we show that the PT kernel in the $b_{3\text{nl}}$ term exactly matches to the solution in a simple coevolution picture between dark matter and halo fluids (see discussion in Sec. II D). Also, this circumstance evidence becomes even much clearer when the solution in coevolution picture is found out to be

consistent with that derived by the Galileon invariants (see Appendix C and similar discussions can be found in [54]). Also we note that Ref. [56] readdress the bias renormalization in terms of the effective field theory (EFT) language and drew the same conclusion.

Then an inevitable question is whether the model can really well describe the halo statistics in N -body simulations. In particular, can the model simultaneously explain the halo power spectrum and the bispectrum which is never achieved in a simple local bias model [46,47]? To answer this question, we fit the model including nonlocal bias terms to the power spectrum, combined with the bispectrum. We here focus on the cross spectra between halos and dark matter which are free from issues such as halo exclusion [82] or stochasticity [61,83,84]. A novel thing in this work is to compare the model for the cross spectrum between halo density and matter momentum. The momentum power spectrum is the essential ingredient in predicting RSD in the so-called distribution function approach as initiated by [64]. We show that the fitting values of b_{3nl} up to a certain k_{\max} (typically, $k_{\max} \lesssim 0.1h/\text{Mpc}$) are in a good agreement for two power spectra, saying that the model seems to be able to explain the power spectra and the bispectrum at the same time. We also explore if the derived values of b_{3nl} are consistent with predictions from the simple coevolution picture (or the local Lagrangian bias) and find as a good agreement as second order tidal bias, b_{s^2} , although the agreement is not perfect.

Our study does indicate that there is no reason to ignore the nonlocal bias terms in predicting the halo statistics at a high accuracy. In fact there have been some evidences which suggests the third-order nonlocal bias term should be included in the literature. For instance, Refs. [68,69] find that they need to introduce two different second-order bias parameters for the halo density-density, b_2^{00} and for the halo density-momentum, b_2^{01} to explain the simulated halo power spectrum. As is already discussed in [68], the difference can be, at least qualitatively, explained by the b_{3nl} term. However, we need to be more careful to analyze the halo-halo statistics by properly taking stochasticity noise and velocity bias into account. Even though many improvements still need to be considered, Ref. [14] applies the model based on our study with nonlocal bias values fixed to be the coevolution predictions to the actual galaxy survey data. One of the reasons why it seems to work is that the authors primarily focus on the anisotropic clustering signal to extract RSD which has larger statistical errors (typically $\sim 10\%$) than the isotropic part (i.e., monopole, typically a few %). Also, additional bias parameters such as the second-order local bias, b_2 , and shot-noise-like bias, N , are conservatively treated as free. In order to extract the shape information from the monopole, however, more refined analysis will be required. We leave it as our future work and hope to report it elsewhere in the near future. Also, there are extensions of the model considered here,

which could make the fit and the comparisons better and extend to higher wave numbers. Let us summarize the key assumptions of our simple coevolution picture again: local Lagrangian initial conditions, a continuity equation for the halo fluid, and no velocity bias. The local Lagrangian initial conditions will be likely to be modified by the presence of initial b_{s^2} and b_{3nl} due to e.g., ellipsoidal collapse [85]. Since we are fitting for the amplitude of these terms, our inferred values are a combination of the initial and dynamical contributions and the agreement with the b_{s^2} , $b_{3nl} \propto (b_1 - 1)$ scaling tells us that the initial contributions are expected to be fairly small. Furthermore, the peak model [86] and studies of proto-haloes in N -body simulations [87] suggest that there is an initial scale dependent linear bias $b_1(k)$, which arises from the dependence of the peak clustering on second derivatives of the field (see [88,89] for a rigorous derivation, and also see [52,62] for subsequent gravitational evolution taken into account). The same calculation also reveals that proto-halo velocities are likely statistically biased on small scales with respect to the underlying matter. Simple considerations for the motions of peaks suggest that these effects are damped by gravitational evolution at linear level. In absence of a well tested description of these effects at the non-linear level, we refrain from taking these effects into account.

Let us make a comment on a related work in Ref. [90]. The authors in Ref. [90] predict the halo-matter power spectrum by fixing bias parameters: the local bias parameters, b_1 and b_2 , are calculated by the peak-background split combined with the non-universal mass function in the excursion set peak formalism [91–93], and the nonlocal bias parameters are fixed with the results of the local Lagrangian bias (i.e., the same as our Sec. II D). In addition, a crucial difference is that they include k^2 -type bias term based on the peak formalism. They claim that their predictions are in a good agreement with simulations including cosmology with massive neutrinos [94] at a few percent level, and the k^2 -type term, which we ignored, is important. This sounds contradictory to our results, but we argue it is not actually the case: in Fig. 9, we observe that our preferred b_{3nl} values are sometimes larger than the coevolution prediction. This means that it is necessary to introduce another component (like k^2 term) to well fit to the simulated data, if the b_{3nl} is fixed to the coevolution prediction. In addition, as is already pointed out in [53] and is shown in Fig. 9, the preferred values of the second-order bias, b_2 and b_{s^2} , are not in a perfect agreement with the simple theoretical predictions. It is interesting to clarify whether the source of this discrepancy comes truly from the k^2 bias or something different, which would require more careful investigation.

As a final remark, we make a comment on future directions of our study. As shown in Fig. 9, our measurements suggests a characteristic dependence of the higher-order local and nonlocal biases on the linear bias b_1 .

This fact implies that there would be a possibility that we could model higher-order bias terms simply in terms of b_1 (or the halo mass M_{halo}), which is an ultimate goal of modeling the halo bias. We believe that our results provide a hint toward a more refined modeling of the nonlinear halo bias without any free parameters. Another legitimate extension of our study is to investigate if the $b_{3\text{nl}}$ term can explain the trispectrum simultaneously. However, Ref. [56] shows that there exists an additional nonlocal term even in the tree-level trispectrum. In addition, the trispectrum analysis requires a gigantic simulation volume to gain ample signal-to-noise ratio. Thus such an analysis would take a rigorous amount of work, even though it is straightforward to do.

ACKNOWLEDGMENTS

We would like to thank Roman Scoccimarro, Ravi Sheth, Kwan Chuen Chan, and Takahiko Matsubara for useful comments and discussions. We acknowledge Vincent Desjacques *et al.* for correspondence regarding their work [90]. S.S. is supported by a Grant-in-Aid for Young Scientists (Start-up) from the Japan Society for the Promotion of Science (JSPS) (No. 25887012). T.B. gratefully acknowledges support from the Institute for Advanced Study through the W.M. Keck Foundation Fund.

APPENDIX A: PERTURBATION THEORY BASICS

In this Appendix we summarize basic equations in perturbation theory.

1. Matter density

A matter density in Fourier space is perturbatively expanded into

$$\begin{aligned} \delta_m(\mathbf{k}) &= \delta_0(\mathbf{k}) + \int \frac{d^3q}{(2\pi)^3} F_S^{(2)}(\mathbf{q}, \mathbf{k} - \mathbf{q}) \delta_0(\mathbf{q}) \delta_0(\mathbf{k} - \mathbf{q}) \\ &+ \int \frac{d^3q_1}{(2\pi)^3} \frac{d^3q_2}{(2\pi)^3} F_S^{(3)}(\mathbf{q}_1, \mathbf{q}_2, \mathbf{k} - \mathbf{q}_1 - \mathbf{q}_2) \\ &\times \delta_0(\mathbf{q}_1) \delta_0(\mathbf{q}_2) \delta_0(\mathbf{k} - \mathbf{q}_1 - \mathbf{q}_2) + \mathcal{O}(\delta_0^4), \end{aligned} \quad (\text{A1})$$

where δ_0 is the linear density perturbation and the symmetrized PT kernels are given by

$$\begin{aligned} F_S^{(2)}(\mathbf{q}_1, \mathbf{q}_2) &= \frac{1}{2} \{F^{(2)}(\mathbf{q}_1, \mathbf{q}_2) + F^{(2)}(\mathbf{q}_2, \mathbf{q}_1)\} \\ &= \frac{5}{7} + \frac{1}{2} \frac{\mathbf{q}_1 \cdot \mathbf{q}_2}{q_1 q_2} \left(\frac{q_1}{q_2} + \frac{q_2}{q_1} \right) + \frac{2}{7} \left(\frac{\mathbf{q}_1 \cdot \mathbf{q}_2}{q_1 q_2} \right)^2, \end{aligned} \quad (\text{A2})$$

$$G_S^{(2)}(\mathbf{q}_1, \mathbf{q}_2) = \frac{3}{7} + \frac{1}{2} \frac{\mathbf{q}_1 \cdot \mathbf{q}_2}{q_1 q_2} \left(\frac{q_1}{q_2} + \frac{q_2}{q_1} \right) + \frac{4}{7} \left(\frac{\mathbf{q}_1 \cdot \mathbf{q}_2}{q_1 q_2} \right)^2, \quad (\text{A3})$$

$$\begin{aligned} F_S^{(3)}(\mathbf{q}_1, \mathbf{q}_2, \mathbf{q}_3) &= \frac{1}{3!} \{F^{(3)}(\mathbf{q}_1, \mathbf{q}_2, \mathbf{q}_3) + \text{cyclic}\} \\ &= \frac{1}{6} \left[\frac{7}{9} \frac{\mathbf{q}_{123} \cdot \mathbf{q}_3}{q_3^2} F_S^{(2)}(\mathbf{q}_1, \mathbf{q}_2) + \left\{ \frac{7}{9} \frac{\mathbf{q}_{123} \cdot (\mathbf{q}_1 + \mathbf{q}_2)}{|\mathbf{q}_1 + \mathbf{q}_2|^2} + \frac{2}{9} \frac{q_{123}^2 \mathbf{q}_3 \cdot (\mathbf{q}_1 + \mathbf{q}_2)}{|\mathbf{q}_1 + \mathbf{q}_2|^2 \cdot q_3^2} \right\} G_S^{(2)}(\mathbf{q}_1, \mathbf{q}_2) \right] \\ &+ \text{cyclic}, \end{aligned} \quad (\text{A4})$$

$$\begin{aligned} G_S^{(3)}(\mathbf{q}_1, \mathbf{q}_2, \mathbf{q}_3) &= \frac{1}{6} \left[\frac{1}{3} \frac{\mathbf{q}_{123} \cdot \mathbf{q}_3}{q_3^2} F_S^{(2)}(\mathbf{q}_1, \mathbf{q}_2) + \left\{ \frac{1}{3} \frac{\mathbf{q}_{123} \cdot (\mathbf{q}_1 + \mathbf{q}_2)}{|\mathbf{q}_1 + \mathbf{q}_2|^2} + \frac{2}{3} \frac{q_{123}^2 \mathbf{q}_3 \cdot (\mathbf{q}_1 + \mathbf{q}_2)}{|\mathbf{q}_1 + \mathbf{q}_2|^2 \cdot q_3^2} \right\} G_S^{(2)}(\mathbf{q}_1, \mathbf{q}_2) \right] \\ &+ \text{cyclic}, \end{aligned} \quad (\text{A5})$$

where $\mathbf{q}_{123} = \mathbf{q}_1 + \mathbf{q}_2 + \mathbf{q}_3$. The unsymmetrized kernels are given by

$$F^{(2)}(\mathbf{q}_1, \mathbf{q}_2) = \frac{5}{7} \alpha(\mathbf{q}_1, \mathbf{q}_2) + \frac{2}{7} \beta(\mathbf{q}_1, \mathbf{q}_2), \quad (\text{A6})$$

$$G^{(2)}(\mathbf{q}_1, \mathbf{q}_2) = \frac{3}{7} \alpha(\mathbf{q}_1, \mathbf{q}_2) + \frac{4}{7} \beta(\mathbf{q}_1, \mathbf{q}_2), \quad (\text{A7})$$

$$\alpha(\mathbf{q}_1, \mathbf{q}_2) = \frac{(\mathbf{q}_1 + \mathbf{q}_2) \cdot \mathbf{q}_1}{q_1^2}, \quad (\text{A8})$$

$$\beta(\mathbf{q}_1, \mathbf{q}_2) = \frac{1}{2} (\mathbf{q}_1 + \mathbf{q}_2)^2 \frac{\mathbf{q}_1 \cdot \mathbf{q}_2}{q_1^2 q_2^2}. \quad (\text{A9})$$

2. Biased tracer's density

Following an ansatz in McDonald and Roy [51], a halo density field (or generally biased tracer) is written as

$$\begin{aligned} \delta_h(\mathbf{x}) &= c_\delta \delta_m(\mathbf{x}) + \frac{1}{2} c_{\delta^2} \delta_m(\mathbf{x})^2 + \frac{1}{2} c_{s^2} s(\mathbf{x})^2 \\ &+ \frac{1}{3!} c_{\delta^3} \delta_m(\mathbf{x})^3 + \frac{1}{2} c_{\delta s^2} \delta_m(\mathbf{x}) s(\mathbf{x})^2 \\ &+ c_\psi \psi(\mathbf{x}) + c_{st} s(\mathbf{x}) t(\mathbf{x}) \\ &+ \frac{1}{3!} c_{s^3} s(\mathbf{x})^3 + c_\epsilon \epsilon + \dots, \end{aligned} \quad (\text{A10})$$

where each independent variable is defined as

$$s_{ij}(\mathbf{x}) \equiv \partial_i \partial_j \phi(\mathbf{x}) - \frac{1}{3} \delta_{ij}^K \delta_m(\mathbf{x}) = \left[\partial_i \partial_j \partial^{-2} - \frac{1}{3} \delta_{ij}^K \right] \delta_m(\mathbf{x}), \quad (\text{A11})$$

$$t_{ij}(\mathbf{x}) \equiv \partial_i v_j - \frac{1}{3} \delta_{ij}^K \theta_m(\mathbf{x}) - s_{ij}(\mathbf{x}) = \left[\partial_i \partial_j \partial^{-2} - \frac{1}{3} \delta_{ij}^K \right] [\theta(\mathbf{x}) - \delta_m(\mathbf{x})], \quad (\text{A12})$$

$$\psi(\mathbf{x}) \equiv [\theta(\mathbf{x}) - \delta_m(\mathbf{x})] - \frac{2}{7} s(\mathbf{x})^2 + \frac{4}{21} \delta_m(\mathbf{x})^2. \quad (\text{A13})$$

Note that t_{ij} is zero at first order, and ψ is zero up to second order. In Fourier space, the halo density contrast is given by

$$\begin{aligned} \delta_h(\mathbf{k}) = & c_\delta \delta_0(\mathbf{k}) + c_\delta \int \frac{d^3 q}{(2\pi)^3} F_S^{(2)}(\mathbf{q}, \mathbf{k} - \mathbf{q}) \delta_0(\mathbf{q}) \delta_0(\mathbf{k} - \mathbf{q}) + \frac{1}{2} c_{\delta^2} \int \frac{d^3 q}{(2\pi)^3} \delta_0(\mathbf{q}) \delta_0(\mathbf{k} - \mathbf{q}) \\ & + \frac{1}{2} c_{s^2} \int \frac{d^3 q}{(2\pi)^3} S^{(2)}(\mathbf{q}, \mathbf{k} - \mathbf{q}) \delta_0(\mathbf{q}) \delta_0(\mathbf{k} - \mathbf{q}) \\ & + c_\delta \int \frac{d^3 q_1}{(2\pi)^3} \frac{d^3 q_2}{(2\pi)^3} F_S^{(3)}(\mathbf{q}_1, \mathbf{q}_2, \mathbf{k} - \mathbf{q}_1 - \mathbf{q}_2) \delta_0(\mathbf{q}_1) \delta_0(\mathbf{q}_2) \delta_0(\mathbf{k} - \mathbf{q}_1 - \mathbf{q}_2) \\ & + c_{\delta^2} \int \frac{d^3 q_1}{(2\pi)^3} \frac{d^3 q_2}{(2\pi)^3} F_S^{(2)}(\mathbf{q}_1, \mathbf{k} - \mathbf{q}_1 - \mathbf{q}_2) \delta_0(\mathbf{q}_1) \delta_0(\mathbf{q}_2) \delta_0(\mathbf{k} - \mathbf{q}_1 - \mathbf{q}_2) \\ & + \frac{1}{3!} c_{\delta^3} \int \frac{d^3 q_1}{(2\pi)^3} \frac{d^3 q_2}{(2\pi)^3} \delta_0(\mathbf{q}_1) \delta_0(\mathbf{q}_2) \delta_0(\mathbf{k} - \mathbf{q}_1 - \mathbf{q}_2) \\ & + c_{s^2} \int \frac{d^3 q_1}{(2\pi)^3} \frac{d^3 q_2}{(2\pi)^3} S^{(2)}(\mathbf{q}_1, \mathbf{k} - \mathbf{q}_1) F_S^{(2)}(\mathbf{q}_2, \mathbf{k} - \mathbf{q}_1 - \mathbf{q}_2) \delta_0(\mathbf{q}_1) \delta_0(\mathbf{q}_2) \delta_0(\mathbf{k} - \mathbf{q}_1 - \mathbf{q}_2) \\ & + \frac{1}{3!} c_{s^3} \int \frac{d^3 q_1}{(2\pi)^3} \frac{d^3 q_2}{(2\pi)^3} S^{(3)}(\mathbf{q}_1, \mathbf{q}_2, \mathbf{k} - \mathbf{q}_1 - \mathbf{q}_2) \delta_0(\mathbf{q}_1) \delta_0(\mathbf{q}_2) \delta_0(\mathbf{k} - \mathbf{q}_1 - \mathbf{q}_2) \\ & + \frac{1}{2} c_{\delta s^2} \int \frac{d^3 q_1}{(2\pi)^3} \frac{d^3 q_2}{(2\pi)^3} S^{(2)}(\mathbf{q}_2, \mathbf{k} - \mathbf{q}_1 - \mathbf{q}_2) \delta_0(\mathbf{q}_1) \delta_0(\mathbf{q}_2) \delta_0(\mathbf{k} - \mathbf{q}_1 - \mathbf{q}_2) \\ & + c_\psi \int \frac{d^3 q_1}{(2\pi)^3} \frac{d^3 q_2}{(2\pi)^3} \{ D_S^{(3)}(\mathbf{q}_1, \mathbf{q}_2, \mathbf{k} - \mathbf{q}_1 - \mathbf{q}_2) - 2F_S^{(2)}(\mathbf{q}_1, \mathbf{k} - \mathbf{q}_1 - \mathbf{q}_2) D_S^{(2)}(\mathbf{q}_2, \mathbf{k} - \mathbf{q}_2) \} \\ & \times \delta_0(\mathbf{q}_1) \delta_0(\mathbf{q}_2) \delta_0(\mathbf{k} - \mathbf{q}_1 - \mathbf{q}_2) \\ & + 2c_{st} \int \frac{d^3 q_1}{(2\pi)^3} \frac{d^3 q_2}{(2\pi)^3} S^{(2)}(\mathbf{q}_1, \mathbf{k} - \mathbf{q}_1) D_S^{(2)}(\mathbf{q}_2, \mathbf{q}_1 - \mathbf{q}_2) \delta_0(\mathbf{q}_1) \delta_0(\mathbf{q}_2) \delta_0(\mathbf{k} - \mathbf{q}_1 - \mathbf{q}_2), \end{aligned} \quad (\text{A14})$$

where

$$S^{(2)}(\mathbf{q}_1, \mathbf{q}_2) = \left(\frac{\mathbf{q}_1 \cdot \mathbf{q}_2}{q_1 q_2} \right)^2 - \frac{1}{3}, \quad (\text{A15})$$

$$S^{(3)}(\mathbf{q}_1, \mathbf{q}_2, \mathbf{q}_3) = \frac{(\mathbf{q}_1 \cdot \mathbf{q}_2)(\mathbf{q}_2 \cdot \mathbf{q}_3)(\mathbf{q}_3 \cdot \mathbf{q}_1)}{q_1^2 q_2^2 q_3^2} - \frac{1}{3} \frac{(\mathbf{q}_1 \cdot \mathbf{q}_2)^2}{q_1^2 q_2^2} - \frac{1}{3} \frac{(\mathbf{q}_2 \cdot \mathbf{q}_3)^2}{q_2^2 q_3^2} - \frac{1}{3} \frac{(\mathbf{q}_3 \cdot \mathbf{q}_1)^2}{q_3^2 q_1^2} + \frac{2}{9}, \quad (\text{A16})$$

$$D^{(N)} \equiv G^{(N)} - F^{(N)}. \quad (\text{A17})$$

3. Distribution function approach

In the Distribution Function approach to model the redshift-space distortion proposed in Ref. [64], the redshift-space power spectrum, $P^S(\mathbf{k})$, is expanded into infinite sum of momentum power spectrum,

$$P^S(\mathbf{k}) = \sum_{LL'} \frac{(-1)^{L'}}{L!L'!} (ik_{\parallel})^{L+L'} P_{LL'}(\mathbf{k}), \quad (\text{A18})$$

where the momentum and its power spectrum are defined by

$$T_{\parallel}^L(\mathbf{x}) \equiv \{1 + \delta(\mathbf{x})\} v_{\parallel}(\mathbf{x})^L, \quad (\text{A19})$$

$$P_{LL'}(\mathbf{k})(2\pi)^3 \delta_D(\mathbf{k} + \mathbf{k}') \equiv \langle T_{\parallel}^L(\mathbf{k}) T_{\parallel}^{L'}(\mathbf{k}') \rangle. \quad (\text{A20})$$

Note that the velocity is defined in units of the Hubble velocity, and we define the velocity dispersion θ so that $\delta = \theta$ in linear regime. The velocity divergence θ is written in Fourier space as

$$v_{\parallel}(\mathbf{k}) = -if \frac{k_{\parallel}}{k^2} \theta(k). \quad (\text{A21})$$

4. Halo-halo power spectrum

The auto power spectrum of halo is similarly given by

$$\begin{aligned} P_{00}^{\text{hh}}(k) &= b_1^2 P_{\delta\delta}^{\text{NL}}(k) + 2b_1 b_2 P_{b_2, \delta}(k) + 2b_1 b_{s^2} P_{b_{s^2}, \delta}(k) \\ &+ 2b_1 b_{3\text{nl}} \sigma_3^2(k) P(k) + b_2^2 P_{b_{22}}(k) \\ &+ 2b_2 b_{s^2} P_{b_{2s^2}}(k) + b_{s^2}^2 P_{s_{22}}(k) + N, \end{aligned} \quad (\text{A22})$$

where

$$P_{b_{22}}(k) \equiv \frac{1}{2} \int \frac{d^3 q}{(2\pi)^3} P(q) \{P(|\mathbf{k} - \mathbf{q}|) - P(q)\}, \quad (\text{A23})$$

$$\begin{aligned} P_{b_{2s^2}}(k) &\equiv \frac{1}{2} \int \frac{d^3 q}{(2\pi)^3} P(q) \\ &\times \left\{ P(|\mathbf{k} - \mathbf{q}|) S^{(2)}(\mathbf{q}, \mathbf{k} - \mathbf{q}) - \frac{2}{3} P(q) \right\}, \end{aligned} \quad (\text{A24})$$

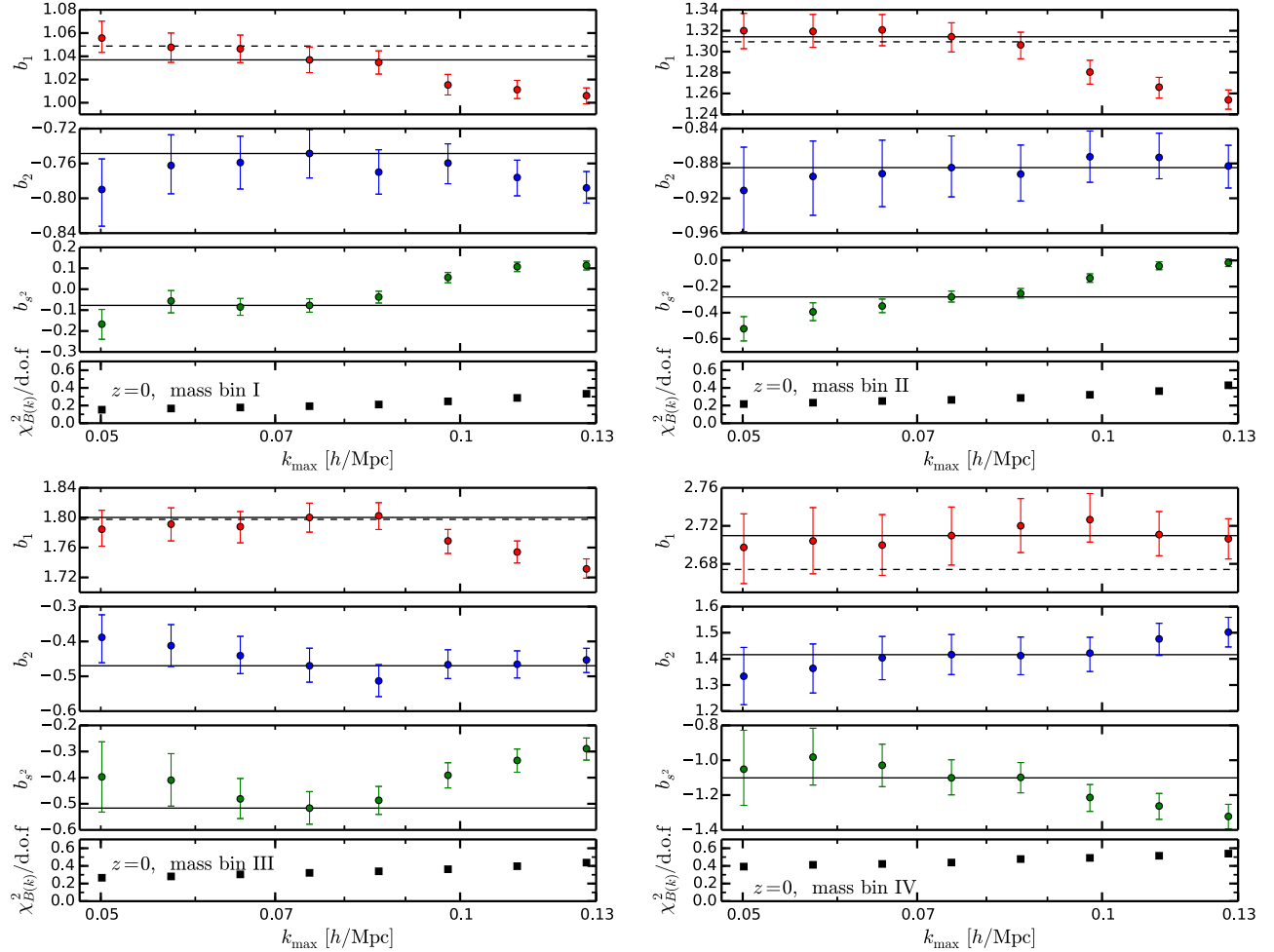
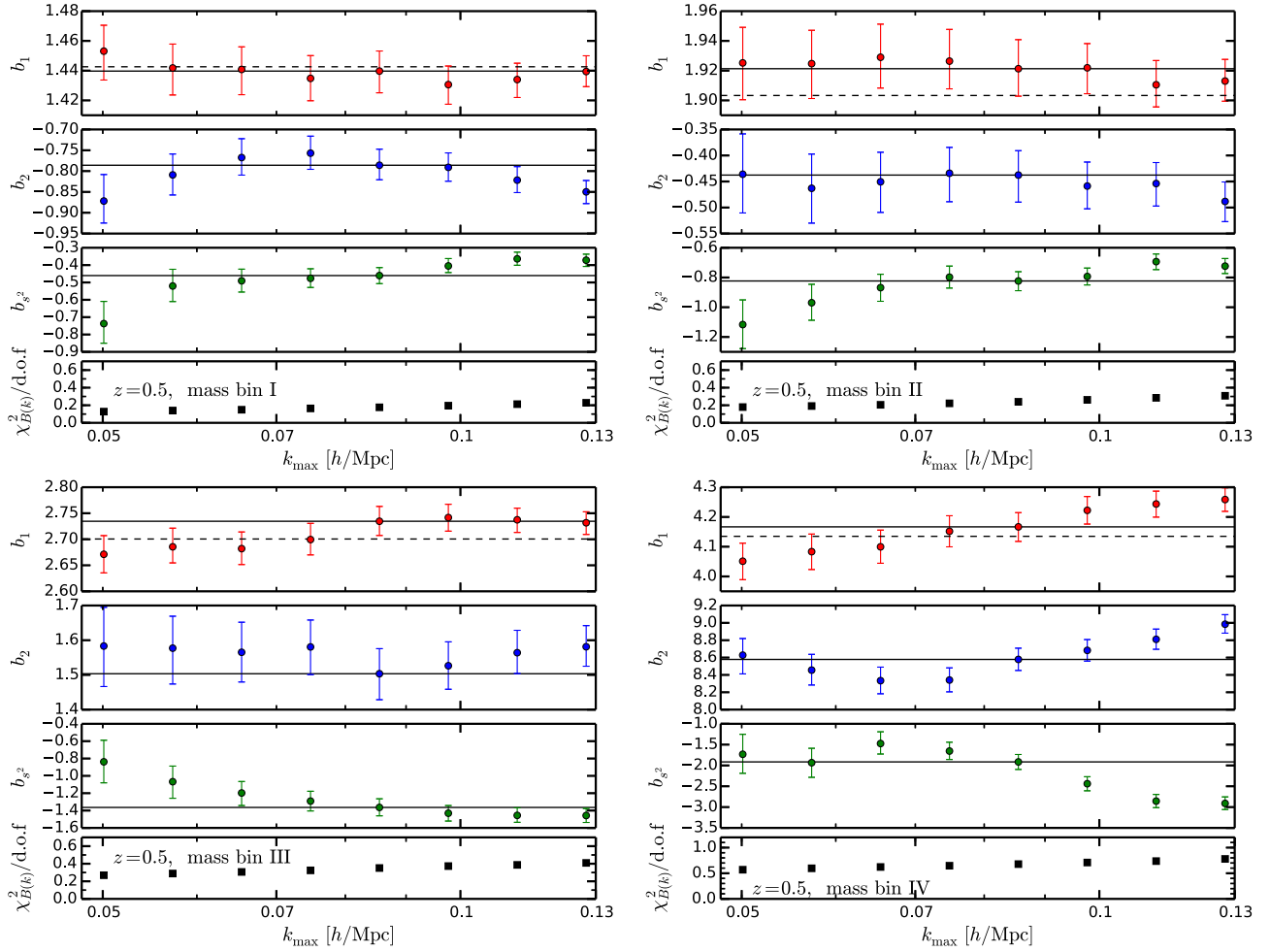


FIG. 10 (color online). The best-fitting values of the bias parameters only from the bispectrum at $z = 0$ as a function k_{max} . Our fiducial choice at $k_{\text{max}, B(k)} = 0.065 h/\text{Mpc}$ is highlighted with a *black solid line*. As a reference, the value of b_1 preferred by joint fitting with the power spectrum is indicated with a *black dashed line*.


 FIG. 11 (color online). Same as Fig. 10, but at $z = 0.5$.

$$P_{bs22}(k) \equiv \frac{1}{2} \int \frac{d^3 q}{(2\pi)^3} P(q) \times \left\{ P(|\mathbf{k}-\mathbf{q}|) S^{(2)}(\mathbf{q}, \mathbf{k}-\mathbf{q})^2 - \frac{4}{9} P(q) \right\}. \quad (\text{A25})$$

Here we subtract the constant terms like $\int d^3 q P(q)^2$ to keep nonlinear corrections vanishing in the limit of $k \rightarrow 0$. Also, cross spectrum between halo density and halo momentum is given by

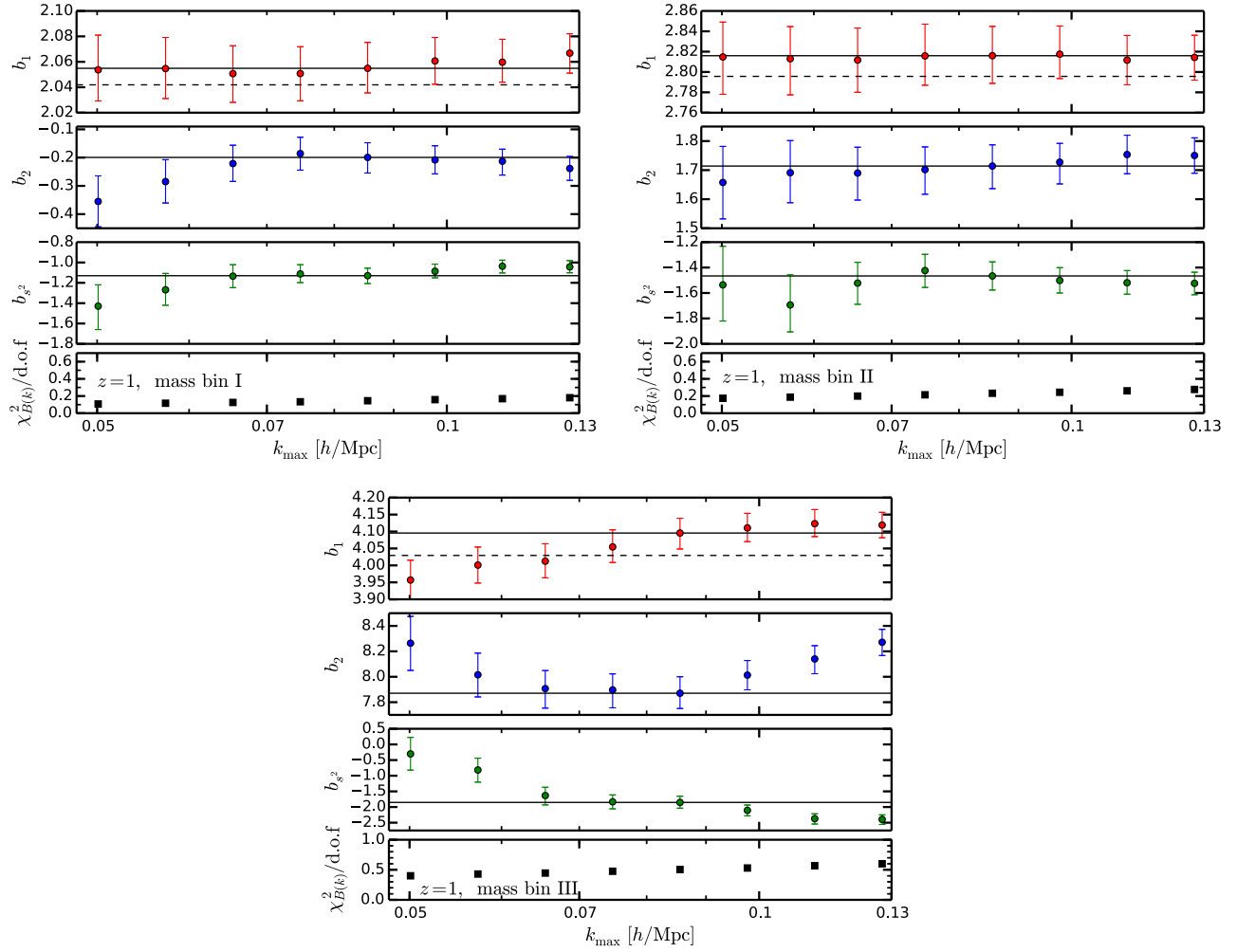
$$\begin{aligned}
 P_{01}^{\text{hh}}(k) &= b_1 f \{ P_{\delta\theta}^{\text{NL}}(k) + B_{b1}(k) \} + b_1 (b_1 - 1) B_{b1}(k) \\
 &+ b_2 \{ P_{b2,\theta}(k) + b_1 B_{b2}(k) \} \\
 &+ b_{s^2} \{ P_{bs2,\theta}(k) + b_1 B_{bs2}(k) \} \\
 &+ b_{3\text{nl}} \sigma_3^2(k) P(k). \quad (\text{A26})
 \end{aligned}$$

APPENDIX B: FITTING BIAS PARAMETERS ONLY AGAINST THE BISPECTRUM

As we discussed in Sec. II C, the bispectrum is useful to access the second-order bias parameters, since the tree-level

bispectrum depends only on the bias parameters up to second order. In other words, it is necessary to carefully investigate the valid range of the tree-level bispectrum. Here we show the fitting results using the bispectrum alone in our simulation. A set of free parameters is (b_1, b_2, b_{s^2}) in this case. Note that this analysis is slightly different from that in previous work [53]: we vary b_1 as a free parameter, while the authors in [53] fixed the value of b_1 taken from the halo-matter power spectrum. Since we intend to combine the power spectrum with the bispectrum and we have already seen that there exists an anticorrelation between b_1 and $b_{3\text{nl}}$ in the joint fit, it is helpful to isolate the information only from the bispectrum.

Figures 10–12 show bias parameters derived at $z = 0, 0.5$ and 1, respectively, from our MCMC fitting as a function of k_{max} . As found in [53], we see non-zero second-order tidal bias b_{s^2} for a variety of halo mass bins and redshifts. In addition the figures show that larger k_{max} results in general deviate more from low k_{max} ones with higher χ^2 values, implying the PT model certainly breaks down at such small scales. Based upon these considerations

FIG. 12 (color online). Same as Fig. 10, but at $z = 1$.

we choose the valid range of the maximum wave number in the bispectrum in a redshift-dependent way: $k_{\max,B(k)} = 0.065(0.075)h/\text{Mpc}$ at $z = 0$ ($z = 0.5$ or 1). Note this choice is fully consistent with the $z = 0$ result in Ref. [53]. Interestingly, this is achieved without adding information on the linear bias b_1 from the power spectrum. In fact the preferred values of b_1 only from the bispectrum tend to more deviate from ones in the joint-fit results at higher mass bins at higher redshift. This issue is also addressed in Figs. 6–8. When the preferred b_1 value from the bispectrum differs from that from the power spectrum, the bias values presented here could be different from those exhibited in the main text.

APPENDIX C: CONSISTENCY CHECK WITH THE GALILEON INVARIANT APPROACH

In Sec. II D we derived solutions up to third order for the simple coevolution equations of dark matter and halo fluids starting from initial condition with purely local bias (i.e., local Lagrangian bias). As a matter of fact such solutions

have been already derived in Ref. [54,95], but the authors took a different route which is based on Galileon symmetry in gravity. In this Appendix we review the Galileon invariant approach and check that this approach is perfectly consistent with ours as expected.

In the Lagrangian picture, gravitational evolution of displacement field is solely governed by the velocity potential, Φ_v , defined by $\theta = \nabla^2 \Phi_v$. Since the halo distribution is a scalar under translations and rotation in three dimensional space, it should be written down in terms of scalar invariants of $\nabla_i \nabla_j \Phi_v$. It is known that there are only three such invariants in three dimensional space, so-called Galileons [96]:

$$\mathcal{G}_1 = \nabla^2 \Phi_v, \quad (\text{C1})$$

$$\mathcal{G}_2 = (\nabla_i \nabla_j \Phi_v)^2 - (\nabla^2 \Phi_v)^2, \quad (\text{C2})$$

$$\mathcal{G}_3 = (\nabla^2 \Phi_v)^3 + 2(\nabla_i \nabla_j \Phi_v)(\nabla_j \nabla_k \Phi_v)(\nabla_k \nabla_i \Phi_v) - 3(\nabla_i \nabla_j \Phi_v)^2 \nabla^2 \Phi_v. \quad (\text{C3})$$

Reference [54] rewrote the coevolution equations and derived the solutions in terms of Galileons. Since their approach solves the exactly same gravity system, it is quite natural to achieve the consistent solution with what we derived in Sec. II D. Note that this approach does not hold if there exists a velocity bias, since relative motion between dark matter and halo fluids obviously breaks down the Galileon symmetry. Let us first begin with the second-order solution which is obtained as ($\epsilon = 1$ and $y \rightarrow \infty$ in Eq. (95) in Ref. [54])

$$\delta_h^{(2)} = b_1^E \delta^{(2)} + \frac{b_2^L}{2} \delta^{(1)2} - \frac{2}{7} b_1^L \mathcal{G}_2^{(2)}(\Phi_v), \quad (\text{C4})$$

where $\mathcal{G}_2^{(2)}(\Phi_v)$ in Fourier space is

$$\mathcal{G}_2^{(2)}(\Phi_v)(\mathbf{q}_1, \mathbf{q}_2) = \frac{(\mathbf{q}_1 \cdot \mathbf{q}_2)^2}{q_1^2 q_2^2} - 1. \quad (\text{C5})$$

$$\begin{aligned} \mathcal{G}_2^{(3)}(\Phi_v)(\mathbf{q}_1, \mathbf{q}_2, \mathbf{q}_3) = & 2 \left[\frac{\{\mathbf{q}_1 \cdot (\mathbf{q}_2 + \mathbf{q}_3)\}^2}{q_1^2} \left\{ \frac{1}{2} \frac{\mathbf{q}_2 \cdot \mathbf{q}_3}{q_2^2 q_3^2} - \frac{3}{7} \frac{1}{(\mathbf{q}_2 + \mathbf{q}_3)^2} \left[\frac{(\mathbf{q}_2 \cdot \mathbf{q}_3)^2}{q_2^2 q_3^2} - 1 \right] \right\} \right. \\ & \left. - (\mathbf{q}_2 + \mathbf{q}_3)^2 \left\{ \frac{1}{2} \frac{\mathbf{q}_2 \cdot \mathbf{q}_3}{q_2^2 q_3^2} - \frac{3}{7} \frac{1}{(\mathbf{q}_2 + \mathbf{q}_3)^2} \left[\frac{(\mathbf{q}_2 \cdot \mathbf{q}_3)^2}{q_2^2 q_3^2} - 1 \right] \right\} \right] \delta_0(\mathbf{q}_1) \delta_0(\mathbf{q}_2) \delta_0(\mathbf{q}_3). \end{aligned} \quad (\text{C7})$$

A tedious and long calculation shows that this solution exactly matches Eq. (40). Here also $b_3^E = -(708/567)b_1^L - (13/7)b_2^L + b_3^L$ is helpful to find the match. As discussed in Ref. [54] (see also [56]), it is not necessary to start with Eq. (A14) and there are duplicated terms in third-order terms in Eq. (A14). However, this fact does not alter our discussion since all the nonlocal third-order terms can be summarized into the $b_{3\text{nl}}$ term anyway as shown in Sec. II D or in Ref. [51].

APPENDIX D: PREDICTING LOCAL BIAS PARAMETERS FROM THE PEAK-BACKGROUND SPLIT WITH THE UNIVERSAL MASS FUNCTION

In this Appendix, we summarize how to predict the local bias parameters, b_1 and b_2 , on the basis of a simple peak-background split [86] combined with the universal halo mass function. For this purpose we here adopt the Sheth-Tormen (ST) fitting formula for the universal mass function [44]. The similar contents can be found in the literature (see e.g., [97]) and, this Appendix follows the notation in Refs. [53,98,99].

The universal halo mass function basically assume that it depends only the peak height ν defined as

$$\nu(R, z) = \frac{\delta_c^2}{\sigma(R, z)^2}, \quad (\text{D1})$$

where we set the density threshold δ_c to be 1.686 based on the spherical collapse, and the variance of the matter fluctuation field smoothed over the scale R is given by

Thus the Fourier-transformed version of Eq. (C4) matches Eq. (37). Note that the simple relation between Eulerian and Lagrangian bias, $b_2^E = b_2^L + (8/21)b_1^L$ is used. Likewise the third-order solution is given by ($\epsilon = 1$ and $y \rightarrow \infty$ in Eq. (99) in Ref. [54])

$$\begin{aligned} \delta_h^{(3)} = & b_1^E \delta^{(3)} + b_2^L \delta^{(1)} \delta^{L(2)} + \left(\frac{b_3^L}{6} - \frac{b_2^L}{2} \right) \delta^{(1)3} \\ & - \frac{2}{7} b_2^L \delta^{(1)} \mathcal{G}_2^{(2)}(\Phi_v) - \frac{22}{126} b_1^L \nabla[\mathcal{G}_2^{(2)}(\Phi_v) \mathbf{v}^{(1)}] \\ & - \frac{1}{9} b_1^L \mathcal{G}_2^{(3)}(\Phi_v), \end{aligned} \quad (\text{C6})$$

where $\delta^{L(2)} = \delta^{(1)2} + \mathbf{v}^{(1)} \cdot \nabla \delta^{(1)} + 2\mathcal{G}_2^{(2)}/7$, and the (unsymmetrized) third-order part of the second-order Galileon is written in Fourier space as

$$\sigma^2(R, z) = \int \frac{k^2 dk}{2\pi^2} P(k, z) |W(kR)|^2, \quad (\text{D2})$$

with $W(kR)$ being the top-hat window function, i.e., $W(x) = 3(\sin x - x \cos x)/x^3$. Here the Lagrangian radius R is simply connected to the halo mass as $R = \{3M/(4\pi\bar{\rho}_m)\}^{1/3}$. Note that R does not depend on redshift. In the peak-background split, the local Lagrangian bias parameters are written down as

$$b_1^L(M, z) = -\frac{1}{\bar{n}} \frac{2\nu}{\delta_c} \frac{\partial n}{\partial \nu}, \quad (\text{D3})$$

$$b_2^L(M, z) = \frac{4\nu^2}{\bar{n}} \frac{\partial^2 n}{\delta_c^2 \partial \nu^2} + \frac{2\nu}{\bar{n}} \frac{\partial n}{\delta_c^2 \partial \nu}. \quad (\text{D4})$$

In the case of the ST mass function, the derivatives are analytically expressed by

$$\frac{1}{\bar{n}} \frac{\partial n}{\partial \nu} = -\frac{q\nu - 1}{2\nu} - \frac{p}{\nu\{1 + (q\nu)^p\}}, \quad (\text{D5})$$

$$\frac{1}{\bar{n}} \frac{\partial^2 n}{\partial \nu^2} = \frac{p^2 + \nu pq}{\nu^2\{1 + (q\nu)^p\}} + \frac{(q\nu)^2 - 2q\nu - 1}{4\nu^2}, \quad (\text{D6})$$

where we adopt $(p, q) = (0.15, 0.75)$. Finally we obtain the Eulerian local bias parameters using Eqs. (36) and (38).

- [1] E. Komatsu, J. Dunkley, M. R.olta, C. L. Bennett, B. Gold, G. Hinshaw, N. Jarosik, D. Larson, M. Limon, L. Page, D. N. Spergel, M. Halpern, R. S. Hill, A. Kogut, S. S. Meyer, G. S. Tucker, J. L. Weiland, E. Wollack, and E. L. Wright, *Astrophys. J. Suppl. Ser.* **180**, 330 (2009).
- [2] E. Komatsu *et al.*, *Astrophys. J. Suppl. Ser.* **192**, 18 (2011).
- [3] G. Hinshaw *et al.*, *Astrophys. J. Suppl. Ser.* **208**, 19 (2013).
- [4] Planck Collaboration, P. A. R. Ade, N. Aghanim, C. Armitage-Caplan, M. Arnaud, M. Ashdown, F. Atrio-Barandela, J. Aumont, C. Baccigalupi, A. J. Banday *et al.*, *Astron. Astrophys.* **571**, A16 (2014).
- [5] D. H. Weinberg, M. J. Mortonson, D. J. Eisenstein, C. Hirata, A. G. Riess, and E. Rozo, *Phys. Rep.* **530**, 87 (2013).
- [6] F. Bernardeau, S. Colombi, E. Gaztañaga, and R. Scoccimarro, *Phys. Rep.* **367**, 1 (2002).
- [7] D. Schlegel, M. White, and D. Eisenstein, [arXiv:0902.4680](https://arxiv.org/abs/0902.4680).
- [8] D. J. Eisenstein, D. H. Weinberg, E. Agol, H. Aihara, C. Allende Prieto, S. F. Anderson, J. A. Arns, É. Aubourg, S. Bailey, E. Balbinot *et al.*, *Astron. J.* **142**, 72 (2011).
- [9] M. J. Drinkwater *et al.*, *Mon. Not. R. Astron. Soc.* **401**, 1429 (2010).
- [10] L. Anderson *et al.*, *Mon. Not. R. Astron. Soc.* **439**, 83 (2014).
- [11] B. A. Reid *et al.*, *Mon. Not. R. Astron. Soc.* **426**, 2719 (2012).
- [12] L. Anderson *et al.*, *Mon. Not. R. Astron. Soc.* **441**, 24 (2014).
- [13] L. Samushia *et al.*, *Mon. Not. R. Astron. Soc.* **439**, 3504 (2014).
- [14] F. Beutler, S. Saito, H.-J. Seo, J. Brinkmann, K. S. Dawson, D. J. Eisenstein, A. Font-Ribera, S. Ho, C. K. McBride, F. Montesano, W. J. Percival, A. J. Ross, N. P. Ross, L. Samushia, D. J. Schlegel, A. G. Sánchez, J. L. Tinker, and B. A. Weaver, *Mon. Not. R. Astron. Soc.* **443**, 1065 (2014).
- [15] F. Beutler, S. Saito, J. R. Brownstein, C.-H. Chuang, A. J. Cuesta, W. J. Percival, A. J. Ross, N. P. Ross, D. P. Schneider, L. Samushia, A. G. Sánchez, H.-J. Seo, J. L. Tinker, C. Wagner, and B. A. Weaver, *Mon. Not. R. Astron. Soc.* **444**, 3501 (2014).
- [16] G.-B. Zhao, S. Saito, W. J. Percival, A. J. Ross, F. Montesano, M. Viel, D. P. Schneider, D. J. Ernst, M. Manera, J. Miralda-Escude, N. P. Ross, L. Samushia, A. G. Sanchez, M. E. C. Swanson, D. Thomas, R. Tojeiro, C. Yeche, and D. G. York, *Mon. Not. R. Astron. Soc.* **436**, 2038 (2013).
- [17] B. A. Reid, H.-J. Seo, A. Leauthaud, J. L. Tinker, and M. White, *Mon. Not. R. Astron. Soc.* **444**, 476 (2014).
- [18] C. Blake *et al.*, *Mon. Not. R. Astron. Soc.* **415**, 2876 (2011).
- [19] C. Blake *et al.*, *Mon. Not. R. Astron. Soc.* **415**, 2892 (2011).
- [20] C. Blake *et al.*, *Mon. Not. R. Astron. Soc.* **418**, 1707 (2011).
- [21] C. Blake *et al.*, [arXiv:1108.2637](https://arxiv.org/abs/1108.2637).
- [22] C. Blake *et al.*, *Mon. Not. R. Astron. Soc.* **425**, 405 (2012).
- [23] C. Contreras, *Mon. Not. R. Astron. Soc.* **430**, 924 (2013).
- [24] M. I. Scrimgeour *et al.*, *Mon. Not. R. Astron. Soc.* **425**, 116 (2012).
- [25] M. Takada *et al.*, [arXiv:1206.0737](https://arxiv.org/abs/1206.0737).
- [26] J. J. Adams *et al.*, *Astrophys. J. Suppl. Ser.* **192**, 5 (2011).
- [27] M. Levi, C. Bebek, T. Beers, R. Blum, R. Cahn, D. Eisenstein, B. Flaugher, K. Honscheid, R. Kron, O. Lahav, P. McDonald, N. Roe, D. Schlegel, and the DESI Collaboration, [arXiv:1308.0847](https://arxiv.org/abs/1308.0847).
- [28] R. Laureijs, J. Amiaux, S. Arduini, J. Auguères, J. Brinchmann, R. Cole, M. Cropper, C. Dabin, L. Duvet, A. Ealet *et al.*, [arXiv:1110.3193](https://arxiv.org/abs/1110.3193).
- [29] A. Cooray and R. Sheth, *Phys. Rep.* **372**, 1 (2002).
- [30] U. Seljak, *Mon. Not. R. Astron. Soc.* **318**, 203 (2000).
- [31] P. S. Behroozi, C. Conroy, and R. H. Wechsler, *Astrophys. J.* **717**, 379 (2010).
- [32] R. M. Reddick, R. H. Wechsler, J. L. Tinker, and P. S. Behroozi, *Astrophys. J.* **771**, 30 (2013).
- [33] A. P. Hearin and D. F. Watson, *Mon. Not. R. Astron. Soc.* **435**, 1313 (2013).
- [34] A. R. Zentner, A. P. Hearin, and F. C. van den Bosch, *Mon. Not. R. Astron. Soc.* **443**, 3044 (2014).
- [35] A. Leauthaud, J. Tinker, P. S. Behroozi, M. T. Busha, and R. H. Wechsler, *Astrophys. J.* **738**, 45 (2011).
- [36] J. L. Tinker, A. Leauthaud, K. Bundy, M. R. George, P. Behroozi, R. Massey, J. Rhodes, and R. H. Wechsler, *Astrophys. J.* **778**, 93 (2013).
- [37] H. Guo, Z. Zheng, I. Zehavi, H. Xu, D. J. Eisenstein, D. H. Weinberg, N. A. Bahcall, A. A. Berlind, J. Comparat, C. K. McBride, A. J. Ross, D. P. Schneider, R. A. Skibba, M. E. C. Swanson, J. L. Tinker, R. Tojeiro, and D. A. Wake, *Mon. Not. R. Astron. Soc.* **441**, 2398 (2014).
- [38] S. Cole, *Mon. Not. R. Astron. Soc.* **362**, 505 (2005).
- [39] M. Tegmark *et al.*, *Phys. Rev. D* **74**, 123507 (2006).
- [40] K. Yamamoto, G. Nakamura, G. Hütsi, T. Narikawa, and T. Sato, *Phys. Rev. D* **81**, 103517 (2010).
- [41] A. Oka, S. Saito, T. Nishimichi, A. Taruya, and K. Yamamoto, *Mon. Not. R. Astron. Soc.* **439**, 2515 (2014).
- [42] N. Kaiser, *Astrophys. J.* **284**, L9 (1984).
- [43] J. N. Fry and E. Gaztanaga, *Astrophys. J.* **413**, 447 (1993).
- [44] R. K. Sheth and G. Tormen, *Mon. Not. R. Astron. Soc.* **308**, 119 (1999).
- [45] J. Tinker, A. V. Kravtsov, A. Klypin, K. Abazajian, M. Warren, G. Yepes, S. Gottlöber, and D. E. Holz, *Astrophys. J.* **688**, 709 (2008).
- [46] J. E. Pollack, R. E. Smith, and C. Porciani, *Mon. Not. R. Astron. Soc.* **420**, 3469 (2012).
- [47] J. E. Pollack, R. E. Smith, and C. Porciani, *Mon. Not. R. Astron. Soc.* **440**, 555 (2014).
- [48] D. Jeong and E. Komatsu, *Astrophys. J.* **691**, 569 (2009).
- [49] S. Saito, M. Takada, and A. Taruya, *Phys. Rev. D* **83**, 043529 (2011).
- [50] A. J. Nishizawa, M. Takada, and T. Nishimichi, *Mon. Not. R. Astron. Soc.* **433**, 209 (2013).
- [51] P. McDonald and A. Roy, *J. Cosmol. Astropart. Phys.* **8** (2009) 20.
- [52] T. Matsubara, *Phys. Rev. D* **83**, 083518 (2011).
- [53] T. Baldauf, U. Seljak, V. Desjacques, and P. McDonald, *Phys. Rev. D* **86**, 083540 (2012).
- [54] K. C. Chan, R. Scoccimarro, and R. K. Sheth, *Phys. Rev. D* **85**, 083509 (2012).
- [55] P. McDonald, *Phys. Rev. D* **74**, 103512 (2006).
- [56] V. Assassi, D. Baumann, D. Green, and M. Zaldarriaga, *J. Cosmol. Astropart. Phys.* **8** (2014) 056.
- [57] A. Kehagias, J. Noreña, H. Perrier, and A. Riotto, *Nucl. Phys.* **B883**, 83 (2014).
- [58] U. Seljak, N. Hamaus, and V. Desjacques, *Phys. Rev. Lett.* **103**, 091303 (2009).

- [59] F.-S. Kitaura, G. Yepes, and F. Prada, *Mon. Not. R. Astron. Soc.* **439**, L21 (2014).
- [60] W. J. Percival and B. M. Schäfer, *Mon. Not. R. Astron. Soc.* **385**, L78 (2008).
- [61] V. Desjacques and R. K. Sheth, *Phys. Rev. D* **81**, 023526 (2010).
- [62] V. Desjacques, M. Crocce, R. Scoccimarro, and R. K. Sheth, *Phys. Rev. D* **82**, 103529 (2010).
- [63] T. Baldauf, V. Desjacques, and U. Seljak, [arXiv:1405.5885](https://arxiv.org/abs/1405.5885).
- [64] U. Seljak and P. McDonald, *J. Cosmol. Astropart. Phys.* **11** (2011) 039.
- [65] T. Okumura, U. Seljak, and V. Desjacques, *J. Cosmol. Astropart. Phys.* **11** (2012) 014.
- [66] T. Okumura, U. Seljak, P. McDonald, and V. Desjacques, *J. Cosmol. Astropart. Phys.* **2** (2012) 010.
- [67] Z. Vlah, U. Seljak, P. McDonald, T. Okumura, and T. Baldauf, *J. Cosmol. Astropart. Phys.* **11** (2012) 009.
- [68] Z. Vlah, U. Seljak, T. Okumura, and V. Desjacques, *J. Cosmol. Astropart. Phys.* **10** (2013) 053.
- [69] J. Blazek, U. Seljak, Z. Vlah, and T. Okumura, *J. Cosmol. Astropart. Phys.* **4** (2014) 001.
- [70] T. Matsubara, *Phys. Rev. D* **77**, 063530 (2008).
- [71] A. Taruya, T. Nishimichi, and S. Saito, *Phys. Rev. D* **82**, 063522 (2010).
- [72] J. N. Fry, *Astrophys. J.* **461**, L65 (1996).
- [73] A. Taruya, *Astrophys. J.* **537**, 37 (2000).
- [74] L. Hui and K. P. Parfrey, *Phys. Rev. D* **77**, 043527 (2008).
- [75] P. Catelan, F. Lucchin, S. Matarrese, and C. Porciani, *Mon. Not. R. Astron. Soc.* **297**, 692 (1998).
- [76] V. Springel, *Mon. Not. R. Astron. Soc.* **364**, 1105 (2005).
- [77] V. Desjacques, U. Seljak, and I. T. Iliev, *Mon. Not. R. Astron. Soc.* **396**, 85 (2009).
- [78] W. J. Percival *et al.*, *Mon. Not. R. Astron. Soc.* **439**, 2531 (2014).
- [79] A. Lewis and S. Bridle, *Phys. Rev. D* **66**, 103511 (2002).
- [80] J. Carlson, M. White, and N. Padmanabhan, *Phys. Rev. D* **80**, 043531 (2009).
- [81] T. Nishimichi, A. Shirata, A. Taruya, K. Yahata, S. Saito, Y. Suto, R. Takahashi, N. Yoshida, T. Matsubara, N. Sugiyama, I. Kayo, Y. Jing, and K. Yoshikawa, *Publ. Astron. Soc. Jpn.* **61**, 321 (2009).
- [82] T. Baldauf, U. Seljak, R. E. Smith, N. Hamaus, and V. Desjacques, *Phys. Rev. D* **88**, 083507 (2013).
- [83] N. Hamaus, U. Seljak, and V. Desjacques, *Phys. Rev. D* **86**, 103513 (2012).
- [84] M. Sato and T. Matsubara, *Phys. Rev. D* **87**, 123523 (2013).
- [85] R. K. Sheth, K. C. Chan, and R. Scoccimarro, *Phys. Rev. D* **87**, 083002 (2013).
- [86] J. M. Bardeen, J. R. Bond, N. Kaiser, and A. S. Szalay, *Astrophys. J.* **304**, 15 (1986).
- [87] A. Elia, A. D. Ludlow, and C. Porciani, *Mon. Not. R. Astron. Soc.* **421**, 3472 (2012).
- [88] V. Desjacques, *Phys. Rev. D* **78**, 103503 (2008).
- [89] F. Schmidt, D. Jeong, and V. Desjacques, *Phys. Rev. D* **88**, 023515 (2013).
- [90] M. Biagetti, V. Desjacques, A. Kehagias, and A. Riotto, *Phys. Rev. D* **90**, 045022 (2014).
- [91] M. Musso, A. Paranjape, and R. K. Sheth, *Mon. Not. R. Astron. Soc.* **427**, 3145 (2012).
- [92] A. Paranjape, R. K. Sheth, and V. Desjacques, *Mon. Not. R. Astron. Soc.* **431**, 1503 (2013).
- [93] A. Paranjape, E. Sefusatti, K. C. Chan, V. Desjacques, P. Monaco, and R. K. Sheth, *Mon. Not. R. Astron. Soc.* **436**, 449 (2013).
- [94] F. Villaescusa-Navarro, F. Marulli, M. Viel, E. Branchini, E. Castorina, E. Sefusatti, and S. Saito, *J. Cosmol. Astropart. Phys.* **3** (2014) 011.
- [95] Reference [73] has already derived such solutions in an exactly same way with ours, but investigated nonlocal terms in terms of stochastic bias in the halo-halo power spectrum.
- [96] A. Nicolis, R. Rattazzi, and E. Trincherini, *Phys. Rev. D* **79**, 064036 (2009).
- [97] S. Saito, M. Takada, and A. Taruya, *Phys. Rev. D* **80**, 083528 (2009).
- [98] T. Baldauf, U. Seljak, and L. Senatore, *J. Cosmol. Astropart. Phys.* **4** (2011) 6.
- [99] A. Slosar, C. Hirata, U. Seljak, S. Ho, and N. Padmanabhan, *J. Cosmol. Astropart. Phys.* **8** (2008) 031.